Modulation of the immune system for treatment of atherosclerosis

Schaftenaar, F.H.

Immunoproteasomal inhibition with ONX-0914 attenuates atherosclerosis and reduces white adipose tissue mass and metabolic syndrome

F.H. Schaftenaar[1*], A.D. van Dam[2], G. de Bruin[3], J. Amersfoort[1], H. Douna[1], M.J. Kröner[1], P.J. van Santbrink[1], A.C. Foks[1], G.H.M van Puijvelde[1], I. Bot[1], B.I. Florea[3], H.S. Overkleeft[3], P.C.N. Rensen[2], J. Kuiper[1*]

Submitted

[1] Division of BioTherapeutics, Leiden Academic Centre for Drug Research, Leiden, The Netherlands
[2] Department of Medicine, Division of Endocrinology, and Einthoven Laboratory for Experimental Vascular Medicine, Leiden University Medical Center, Leiden, The Netherlands
[3] Leiden Institute of Chemistry, Chemical Biology, Leiden, The Netherlands

Abstract

Atherosclerosis is the major underlying pathology of cardiovascular disease, and is driven by hyperlipidemia and inflammation. Cells of hematopoietic origin, including immune cells, express high levels of the immunoproteasome. Inhibition of immunoproteasomal catalytic subunits LMP7 and LMP2 with ONX-0914 has been shown to have immunosuppressive effects and was effective in treating various autoimmune diseases in preclinical models, while its effects on atherosclerosis have not been studied yet. We found that intraperitoneal ONX-0914 treatment reduced atherosclerosis and dendritic cell levels and activation, and levels of antigen experienced T cells in various immune organs. Additionally, ONX-0914 reduced white adipose tissue (WAT) mass, which surprisingly coincided with neutrophil and macrophage accumulation in WAT. We found that primary mature murine adipocytes express immunoproteasomal subunits and upregulate CCL2 after incubation with ONX-0914, providing a mechanism for ONX-0914 induced immune infiltration. ONX-0914 reduced intestinal triglyceride uptake, which was likely the primary cause of the reduction in WAT mass, as ONX-0914 did not increase energy expenditure or reduce food intake. Intraperitoneal treatment with clodronate liposomes to deplete macrophages abolished the inhibitory effect of ONX-0914 on intestinal lipid uptake, indicating involvement of intraperitoneal macrophages in ONX-0914 mediated lipid uptake reduction. Concomitant with a reduction in WAT mass upon ONX-0914 treatment, we observed improvements in markers of metabolic syndrome, including lowered blood triglyceride levels, insulin levels, and fasting blood glucose. These data indicate that immunoproteasomal inhibition could be a useful tool to treat atherosclerosis, obesity, and metabolic syndrome, major health issues in the developed world.

Introduction

Cardiovascular disease is the most common cause of death in the Western world with atherosclerosis as the most common underlying pathology *(1)*. Atherosclerosis is characterized by lipid deposition in the intima of medium to large sized arteries, which evokes immune infiltration in the vessel wall and inflammation. The inflammatory response in atherosclerosis is characterized by a pro-inflammatory and pathogenic Th1 immune response *(2)*. Current treatment of atherosclerosis has however mainly been focused on treating dyslipidemia in patients, which has led to a decrease in cardiovascular events *(1)* . However, as evidenced by the CANTOS trial, immune modulating treatment combined with lipid management can lead to an additional lowering of the risk for major cardiovascular events *(3, 4)*.

An interesting immune regulator is the immunoproteasome, a proteasome variant mainly basally expressed in cells of hematopoietic origin *(5)* and a variant of the constitutive proteasome which is basally expressed in all cells. Proteasomes are responsible for the degradation of the vast majority of cellular proteins and are involved in regulation of cellular processes via targeted degradation of polyubiquitinated proteins *(5)*. Structurally, proteasomes are comprised of a large barrel-like protein complex, the 20S proteasome, which is formed through axial stacking of two heptameric outer α-rings and two heptameric inner β-rings. Regulatory protein subunits can bind to the α-rings and are responsible for binding and unfolding of client proteins and open up the α-ring, which is otherwise almost completely closed restricting untargeted protein entry into the 20S proteasome *(5)*. Client proteins that enter the proteasome are proteolytically cleaved by the lumen facing active sites of the 3 distinct catalytically active β-subunits present per β-ring, which differ between the different proteasome variants. These catalytic subunits exert caspase-like, trypsin-like, and chymotrypsin-like activities which are executed by the β1, β2 and β5 subunit in the constitutive proteasome respectively, and β1i (LMP2), β2i (MECL-1) and β5i (LMP7) subunit in the immunoproteasome respectively *(6)*.

The constitutive- and immunoproteaosomal catalytic subunits diverge in the amino acids after which they proteolytically cleave proteins, resulting in different protein cleavage products *(7)*. Through these divergent protein cleavage patterns, immunoproteasomes were found superior in the generation of MHC-I epitopes, important for the induction of CD8 T cell responses. IFN-γ promotes the expression of the immunoproteasomal subunits, causing inducible immunoproteaome expression also in cells of non-hematopoietic origin. In addition to the generation of MHC-I epitopes, more recent studies suggest that the immunoproteasome also has a more general pro-inflammatory role, inducing pro-inflammatory gene expression in DCs *(8)*. How immunoproteasomal activity induces this pro-

inflammatory gene expression is still subject of speculation. Several studies using the immunoproteasomal LMP7 and LMP2 specific inhibitor ONX-0914 (formerly known as PR-957) *(9, 10)* have confirmed the pro-inflammatory role of the immunoproteasome and have demonstrated the involvement of the immunoproteasome in regulation of multiple inflammatory processes in different immune in cells *in vitro* and *in vivo*. As such, LMP7 inhibition reduced inflammatory cytokine secretion in PBMCs and T cells *(9, 11)*. Furthermore ONX-0914 was found to impact T cell differentiation, as ONX-0914 inhibited CD4 T cell differentiation towards the pro-inflammatory Th1 and Th17 helper T cells, and promoted differentiation towards Tregs *in vitro (12)*. LMP7 inhibition was also found to affect DC functionality, inhibiting the capacity of DCs to prime T cells *(8)*. In various experimental murine models of auto-immune diseases, such as experimental autoimmune encephalomyelitis (EAE), and arthritis, LMP7 inhibition with ONX-0914 reduced disease severity *(9–17)*.

Since the effects of LMP7 inhibition described thus far are potentially beneficial for the outcome of cardiovascular disease, we studied the effect of ONX-0914 on atherosclerosis in LDLr deficient animals. Our results show that on top of reducing atherosclerosis by altering the innate and adaptive immune response, ONX-0914 treatment reduced intestinal lipid uptake, reduced white adipose tissue mass, and improved markers of metabolic syndrome. Our data indicate that immunoproteasomal inhibition using specific inhibitors may be a highly useful to combat atherosclerosis, obesity, and metabolic syndrome.

Results

ONX-0914 treatment reduces atherosclerosis

Pharmacological inhibition of the immunoproteasomal active subunit LMP7 has reduced inflammation in experimental models of autoimmune diseases, thereby reducing disease severity *(9–17)*. To assess the effect of LMP7 inhibition on atherosclerosis development, 12-14 week old female LDLr$^{-/-}$ mice were treated 3 times weekly with ONX-0914 (10 mg/kg intraperitoneally) for 7 weeks while being fed a Western-type diet (WTD). We analyzed the atherosclerotic lesions in the aortic root (Fig. 1A) and observed a 28.4% reduction (p=0.0054) in lesion size in the ONX-0914 treated group (2.8±0.5 x10^5 µm^2) compared to the vehicle treated group (3.8±0.7 x10^5 µm^2), and a trend towards reduced vessel occlusion (p=0.0975) (Fig. 1B). In addition we analyzed the accumulation of macrophages in the atherosclerotic lesions by immunohistochemistry (Fig. 1C) and found that the macrophage area in the lesions was reduced by 26.6%, but the relative macrophage area in the plaque was not affected upon LMP7 inhibition (Fig. 1D). Furthermore we assessed collagen buildup in the plaque by Masson's trichrome staining (Fig. 1E), and found a reduced absolute collagen area and a trend towards relative collagen content of the plaque (p=0.0538) in the ONX-0914 treated group

(Fig. 1F), which indicates a less progressed plaque phenotype in the ONX-0914 treated group than in the control group.

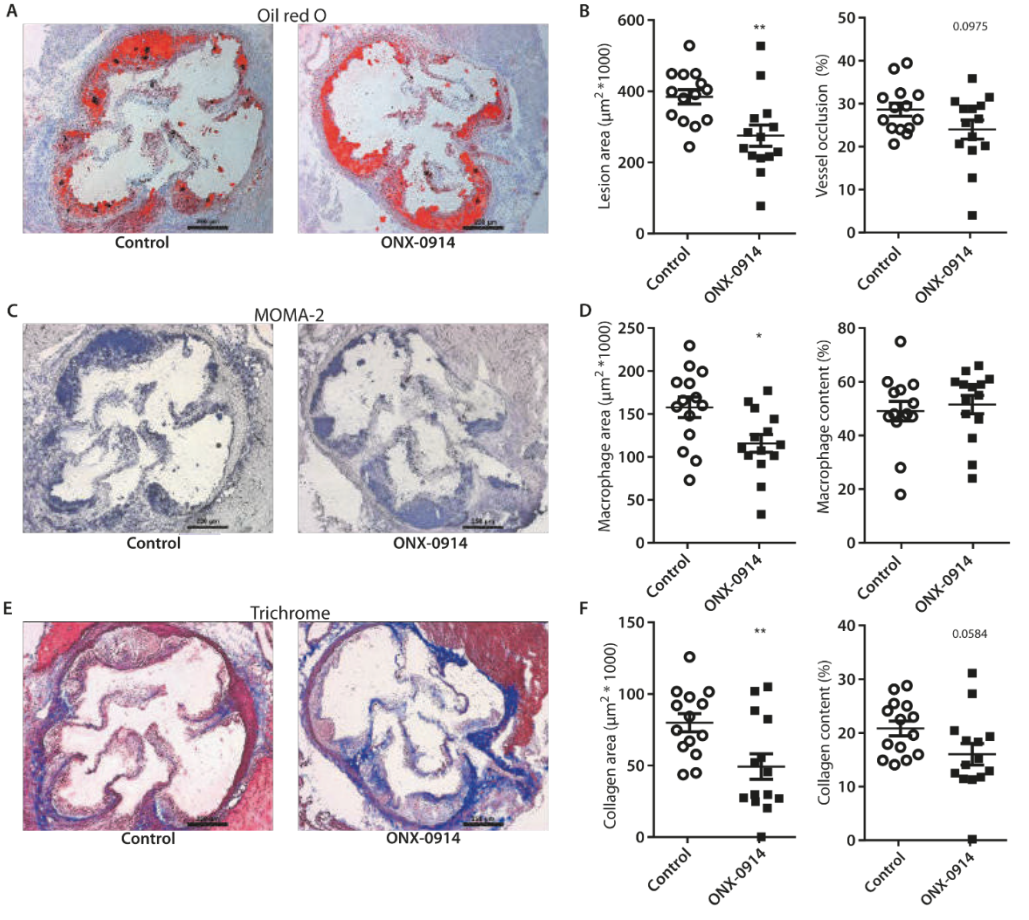

Fig. 1 ***ONX-0914 treatment reduces atherosclerosis in aortic root.*** *12-14 week old Female LDLr$^{-/-}$mice (n=15) were fed WTD for 7 weeks during which ip injections with ONX-0914 (10 mg/kg) or control injections were administered three times weekly.* ***A****) Lipids in the aortic root were stained with oil red O* ***B****) to quantify atherosclerotic lesion area and vessel occlusion.* ***C****) Aortic root sections were immunohistochemically stained using MOMA-2 antibody* ***D****) to determine macrophage area and macrophage content of the plaque.* ***E****) Masson's Trichrome staining was used to assess* ***F****) collagen area and collagen content of the plaque. Expressed as mean ± SEM, unpaired two tailed t-test, *p < 0.05, **p < 0.01.*

ONX-0914 reduces dendritic cell levels and activation

DCs have a pivotal role in atherosclerosis and enhanced activation of dendritic cells induces atherogenesis and mediates CD4 and CD8 T cell activation *(18)*, whereas vaccination with

ApoB100 loaded DCs is atheroprotective and inhibits Th1 and Th2 immunity to ApoB100 *(19, 20)*. It was previously reported that immunoproteasomal deficiency hampers DC functionality *(8)*. Therefore, we assessed the effect of LMP7 inhibition on dendritic cell levels and their activation status with flow cytometry (Fig. 2A) in the spleen, cervical lymph nodes draining from the plaque *(21)* and disease unrelated mesenteric lymph nodes (MLN). ONX-0914 treatment significantly reduced the numbers of conventional CD11c^{+}MHC-II^{+} DCs in all three lymphoid organs (Fig. 2B). Activation of conventional DCs was unaltered in the spleen (Fig. 2C) but slightly lowered in the CLNs (Fig. 2D) and MLNs (Fig. 2E) upon LMP7 inhibition, as judged by the expression of CD86.

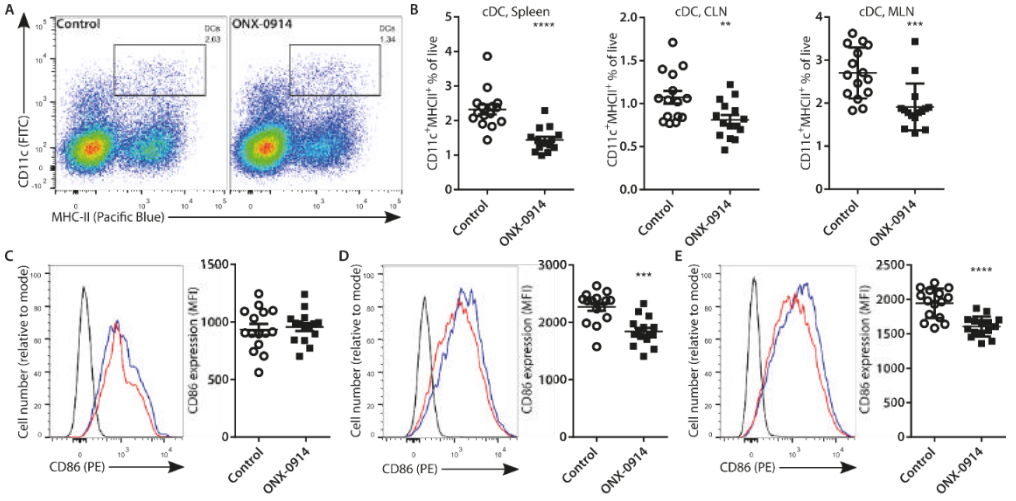

Fig. 2 ***ONX-0914 lowers conventional DC levels and activation in lymphoid organs. A****) Representative flow cytometry plots from spleen, with gating depicted of cDCs based on expression of CD11c and MHC-II.* ***B****) Quantification of cDC levels in spleen, CLN, and MLN. Representative histograms of expression and quantification of median fluorescent intensity (MFI) of CD86 on cDCs in* ***C****) spleen,* ***D****) CLN, and* ***E****) MLN. Expressed as mean ± SEM, unpaired two tailed t-test, **p < 0.01, ***p < 0.001, **** p < 0.0001.*

To assess the direct effect of ONX-0914 on DCs, bone marrow derived DCs (BMDCs) were exposed overnight to ONX-0914 (200 nM) and assessed by flow cytometry (Fig. S1A). ONX-0914 incubation reduced DC viability (Fig. S1B), which could have accounted for the lowered DC levels that were observed in vivo. We did not observe a significant decrease in CD86 expression on DCs *in vitro*, probably due to a low sample size (Fig. S1B). Strikingly, stimulation of BMDCs with LPS reduced cell death caused by ONX-0914 treatment (50-100nM) (Fig. S1C). The observed upregulation in gene expression of constitutive and immunoproteasomal catalytic subunits in LPS-stimulated BMDCs compared to unstimulated DCs (Fig. S1D) likely rendered LPS-stimulated BMDCs less susceptible to ONX-0914 induced cell death. Furthermore, *in vitro* exposure to ONX-0914 (50-100 nM) upregulated expression of the

proteasome subunit β5 in BMDCs (Fig. S1D), much like the previously reported upregulation of the constitutive proteasomal subunit β5 subunit in T cells and B cells treated with ONX-0914 *(22)*. Concomitant with the upregulation of the constitutive β5 subunit, the subunits β1 and β2 were upregulated (Fig. S1D). In contrast to the upregulation of constitutive proteasomal subunits, all immunoproteasomal catalytic subunits and PA28α and PA28β, subunits from the immunoproteasomal PA28αβ regulator, were downregulated by incubation with both concentrations of ONX-0914 in the presence of LPS (Fig. S1D). Since immunoproteasomal deficiency was found to reduce inflammatory gene expression in DCs and DC functionality *(8)*, enhanced expression of constitutive proteasomes over immunoproteasomes in ONX-0914 exposed DCs might explain the suppressive effect of ONX-0914 on DCs. Since pro-inflammatory DCs promote atherogenesis, the observed reduction in DC levels and activation are likely to have contributed to reduced atherosclerosis.

ONX-0914 treatment reduces memory T cell levels

Because atherosclerosis is marked by a pathogenic Th response *(2)*, we assessed whether ONX-0914 treatment skewed T helper differentiation away from Th1 cells towards atheroprotective Tregs, conform previously described *in vitro* and *in vivo* data *(12)*. To assess whether Tregs were induced by ONX-0914 treatment we assessed $CD4^{+}FoxP3^{+}CD25^{+/-}$ cells by flow cytometry (Fig. S2A) in the spleen (Fig. S2B), blood (Fig. S2C), cervical lymph nodes (Fig. S2D) and mesenteric lymph nodes (Fig. S2E), however no enhanced Treg levels were found. To assess whether proliferative capacity of T cells and T cell differentiation were altered by ONX-0914 treatment, splenocyte cultures were stimulated with αCD3 and αCD28, and thymidine incorporation and the cytokine profile in supernatant were assessed. ONX-0914 did not affect thymidine incorporation (Fig. S3A) or IFN-γ, IL-4, IL-17a and IL-10 levels in culture supernatant (Fig. S3B), indicating that splenic T cell proliferation and splenic T cell differentiation towards Th1, Th2, Th17 and Treg were unaffected by ONX-0914 treatment.

In line with these data we did not observe changes in CD4 (Fig. S3C) and CD8 T cell (Fig. S3E) levels, and central memory (Tcm), effector memory (Tem) and naïve (Th0/Tc0) T cell levels after ONX-0914 treatment in the spleen (Fig. S3D/F). Similarly, no differences in the CD4 population were observed in the cervical lymph nodes (Fig. S4A/B). The overall CD8 T cell percentage was, however, significantly increased in the CLN of ONX-0914 treated mice (Fig. S4C) but did not coincide with increases in any of the memory CD8 T cell subpopulations (Fig. S4D). These data suggest that enhanced CD8 T cell levels in the CLN were not the result of enhanced priming of CD8 T cells in the CLN. In mesenteric lymph nodes, however, ONX-0914 treatment caused an overall reduction of CD4 T cell levels (Fig. 3A) and a trend ($p=0.14$) towards reduction in CD4 Tem cells (Fig. 3B). Furthermore LMP7 inhibition reduced CD8 Tem and Tcm cells in the mesenteric lymph nodes (Fig. 3D) while overall CD8 T cell levels were unchanged (Fig. 3C). In the blood overall CD4 and CD8 T cell levels were not significantly

altered (Fig. 3E,G) but CD4 Th0 cell levels were increased (Fig. 3F), and CD8 Tc0 cells were increased coinciding with lowered CD8 Tem cells (Fig. 3H). These data indicate that even though ONX-0914 did not induce Tregs, induction of memory T cells was inhibited by ONX-0914 treatment. This is in line with the previously reported suppressive effect of ONX-0914 on T cells *(12, 22)*. ONX-0914 treatment reduced DC levels and activation, and locally reduced memory CD4 and CD8 T cell levels, which are likely to have contributed to the lowered atherosclerotic lesion size observed upon LMP7 inhibition.

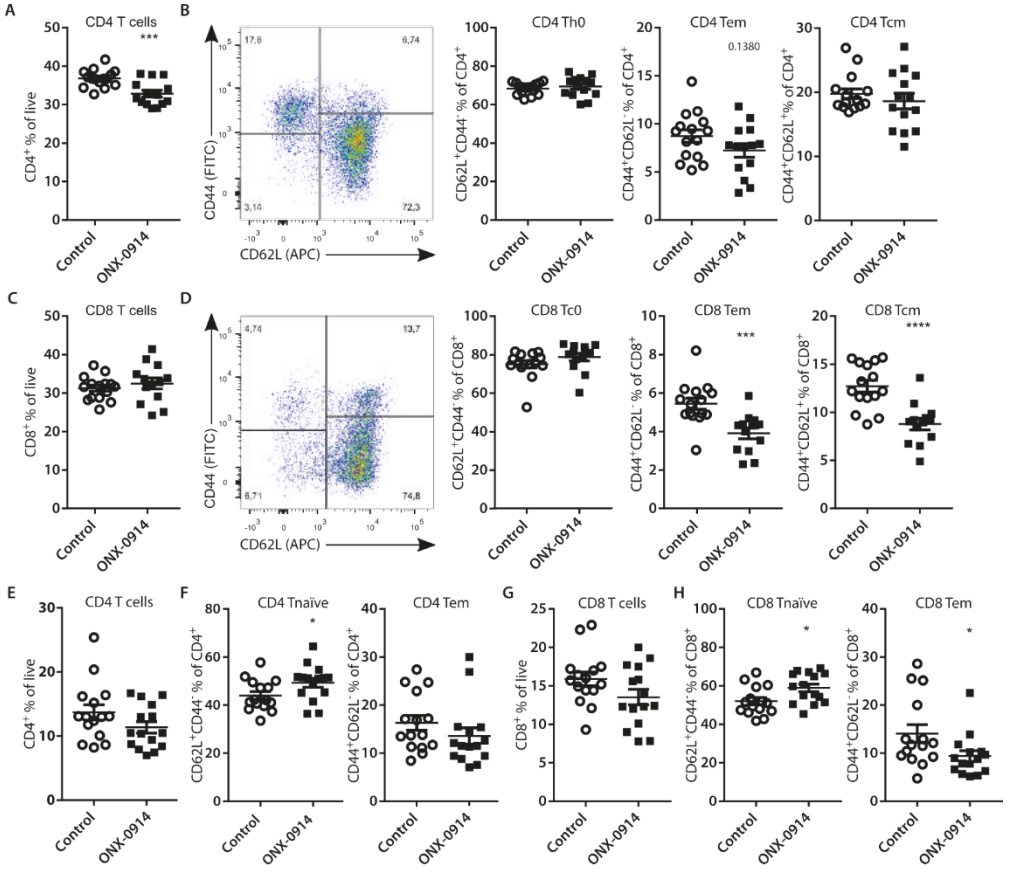

Fig. 3 ***ONX-0914 treatment attenuates maturation of T cells in vivo.*** *Quantification of flow cytometric analysis of* ***A****) CD4 T cell and (C) CD8 T cell content of MLN. Representative flow cytometry plots and quantification of CD62L⁺CD44⁻ naïve, CD44⁺CD62L⁻ effector memory, and CD44⁺CD62L⁺ central memory* ***B****) CD4 T cells and* ***D****) CD8 T cells from MLN. Quantification of* ***E****) CD4 T cells and* ***G****) CD8 T cells and naïve and effector memory* ***F****) CD4 T cells and* ***H****) CD8 T cells in circulation based on flow cytometric analysis. Expressed as mean ± SEM, unpaired two tailed t-test, *p < 0.05, ***p < 0.001, **** p < 0.0001.*

ONX-0914 reduces markers of metabolic syndrome while inducing innate immune activation

Since ONX-0914 was reported to suppress pro-inflammatory cytokine secretion/production *(11, 12)*, a yet additional beneficial effect in the context of atherosclerosis, we assessed the serum cytokine profile in serum of ONX-treated mice using multiplex ELISA. Surprisingly, elevated levels of IL-6 and TNF-α, and a trend towards increased IL-1β levels were detected in serum of ONX-0914 treated mice (Fig. 4A, Fig. S5A for remainder of assessed cytokines). We observed a profound increase in neutrophil levels in blood (Fig. 4B), indicative of innate inflammation, but circulating classical monocyte levels remained stable, and patrolling monocyte populations were reduced (Fig. 4B). Furthermore ONX-0914 treatment reduced body weight (Fig. 4C), virtually depleting gonadal white adipose tissue (gWAT, visual observation), and lowered triglyceride (TG) levels but not cholesterol levels in blood plasma (Fig. 4D).

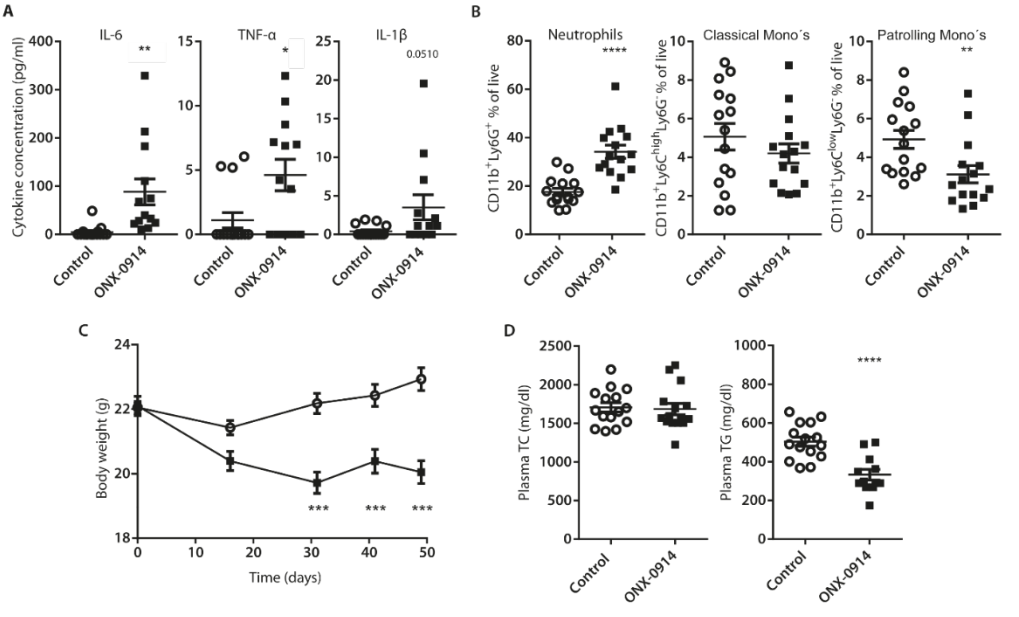

Fig. 4 ***ONX-0914 induces unexpected beneficial metabolic effects and signs of innate inflammation.*** ***A****) Quantification of cytokine levels in blood plasma and* ***B****) quantification of most abundant myeloid cell populations in circulation based on flow cytometric analysis at sacrifice at sacrifice.* ***C****) Body weight over the course of the experiment.* ***D****) Total cholesterol and triglyceride levels in blood plasma at sacrifice. Expressed as mean ± SEM, ABD unpaired two tailed t-test, C two-way repeated measures ANOVA with Holm-Sidak posttest, *p < 0.05, **p < 0.01, ***p < 0.001, **** p < 0.0001.*

Lowered body weight and TG levels as a result of ONX-0914 treatment have not been described previously, therefore we further investigated the mechanisms through which ONX-0914 improved these markers of metabolic syndrome. LMP7 deficiency was previously found to reduce preadipocyte differentiation into mature adipocytes *(23, 24)*. Since ONX-0914 treatment virtually depleted gonadal WAT and reduced body weight, we suspected that ONX-0914 besides possibly affecting preadipocytes, also affected preexistent fat mass. To assess the effect of ONX-0914 on preexisting fat mass, male LDLr$^{-/-}$ mice were fed a WTD for 4 weeks, after which mice were randomized for body weight and age. At this point the baseline group was sacrificed, while the remaining animals were vehicle treated or ONX-0914 treated for 7 weeks.

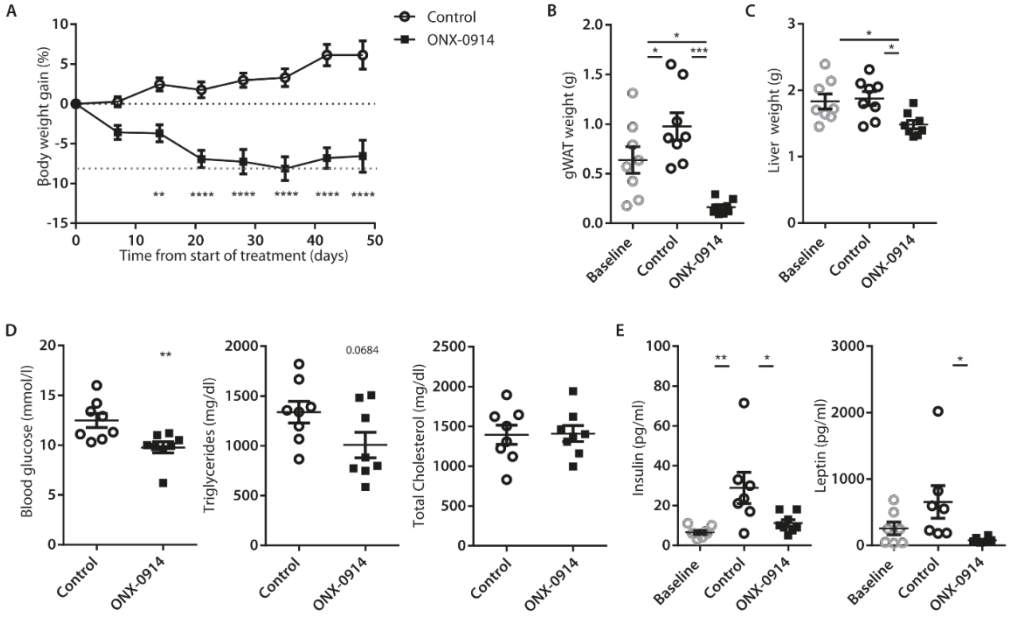

Fig. 5 ***ONX-0914 treatment decreases pre-existing white adipose tissue and improves metabolic parameters.*** *To assess the effect of ONX-0914 treatment on pre-existing fat mass, male 12-14 week old LDLrKO males (n=8) were fed a WTD for 4 weeks. At this point the baseline group was sacrificed and treatment with ONX-0914 (10 mg/kg, three times weekly) or control was commenced and continued for 7 weeks after which the control and treated groups were sacrificed.* ***A****) Gain in body weight of the control and ONX-0914 treated group over the course of treatment.* ***B****) gWAT and* ***C****) Liver weight at time of sacrifice.* ***D****) Blood glucose, triglyceride and total cholesterol levels in blood plasma after 4h fasting after 3.5 weeks of treatment. (****E****) Insulin and leptin concentrations in serum at sacrifice determined with multiplex ELISA. Expressed as mean ± SEM,* ***A****) two-way repeated measures ANOVA with Holm-Sidak posttest* ***BCE****) one-way ANOVA with Holm-Sidak posttest,* ***D****) two tailed t-test, *p < 0.05, **p < 0.01, **** p < 0.0001.*

ONX-0914 treatment resulted in an immune phenotype similar to the previous study in respect to DCs (Fig. S6A-D), CD4 and CD8 T cells (Fig. S7) and neutrophil levels (Fig. S8A/B) compared to vehicle treated mice. Body weight declined from the start of ONX-0914 treatment and stabilized after 4-5 weeks of treatment (Fig. 5A). Consistent with the body weight gain, gWAT weight increased compared to baseline in the vehicle group, and declined nearly 4 fold in ONX-0914 treated animals compared to baseline (Fig. 5B). Liver weight was reduced in ONX-0914 treated animals (Fig. 5C), indicative of less steatosis *(25)*. After 4 weeks of treatment and 40h after ONX-0914 administration, mice were fasted for 4h after which blood glucose, TG and cholesterol levels were determined. Blood glucose was significantly lowered, and a trend towards reduced TG levels was found in the ONX-0914 treated group compared to the vehicle treated group while total cholesterol levels remained stable (Fig. 5D). Furthermore multiplex analysis of metabolism related hormone and cytokine levels in serum after 7 weeks of treatment, revealed increased insulin levels in the vehicle treated group, indicative of insulin resistance, while insulin levels were similar to baseline in ONX-0914 treated animals (Fig. 5E). Leptin levels, correlating with gWAT weight, were lowered in ONX-0914 treated animals compared to vehcicle control group (Fig. 5E). To confirm that weight loss was not due to an off target (hepato)toxic effect of ONX-0914 treatment, we determined the activity of the liver-derived enzymes alanine aminotransaminase (ALAT) and aspartate aminotransferase (ASAT) in blood serum, and hepatic gene expression of Cyp3A11, as readout for PXR activation. We did not observe differences in ALAT and ASAT activities (Fig. S9A) nor in expression of Cyp3A11 (Fig. S9B) between the vehicle and treated group, indicating that ONX-0914 treatment did not induce liver toxicity or PXR activation.

ONX-0914 mediated reduction of white adipose tissue mass is accompanied by neutrophil and macrophage accumulation in gWAT

In humans a homozygous missense mutation in PSMB8, encoding for LMP7, causes lipodystrophy, adipose inflammation and enhanced IL-6 levels *(23)*. Since the phenotype observed in individuals with dysfunctional LMP7 is remarkably similar to the reduced WAT mass and enhanced inflammatory markers we observed when LMP7 (and LMP2) activity in mice was inhibited with ONX-0914, we assessed whether reduced WAT mass was accompanied by immune infiltration in gWAT. To that end we treated mice, which had been fed WTD for 6 weeks already to induce adiposity, with ONX-0914 for 1 week (4 ONX-0914 injections) or 1 day (3 PBS injections followed by 1 ONX-0914 injection), or with vehicle injections (4 PBS injections) to assess the immune response in WAT. 18h after final ip injection, mice were sacrificed and gWAT was isolated. Besides mature adipocytes, WAT is comprised of blood vessels, immune cells, and precursors of mature adipocytes, namely adipose stem cells and preadipocytes, forming the stromal vascular fraction (SVF). To assess the composition of gWAT, gWAT was digested and its SVF was isolated and analyzed by flow

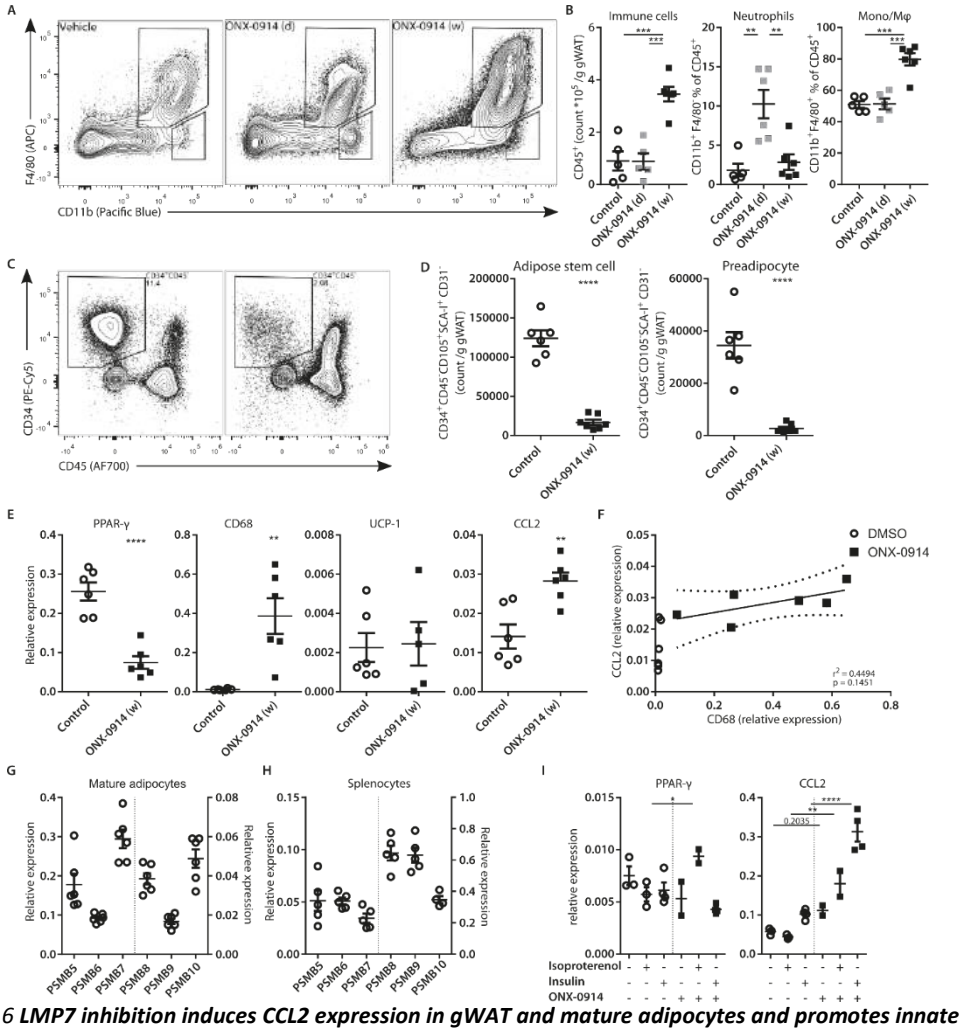

Fig. 6 ***LMP7 inhibition induces CCL2 expression in gWAT and mature adipocytes and promotes innate immune infiltrate. A****) Representative flow cytometry plots of the CD45⁺ immune fraction of the SVF from gWAT, showing the gating for CD11b⁺F4/80⁺ macrophages and CD11b⁺F4/80⁻ neutrophils.* ***B****) Quantification of total immune cells, neutrophils and macrophages in SVF from gWAT.* ***C****) Representative flow cytometry plots for the gating of CD34⁺CD45⁺ cells, containing* ***D****) the SCA-I⁺CD105⁺CD31⁻ adipose stem cells, and SCA-I⁺CD105⁻CD31⁻ preadipocytes.* ***E****) Gene expression of the floating cell fraction from digested gWAT.* ***F****) Correlation analysis between CD68 and CCL2 expression of the floating cell fraction of the ONX-0914 treated group.* ***G****) Gene expression of proteasomal active subunits in freshly isolated mature adipocytes and* ***H****) splenocytes from control treated mice.* ***I****) Gene expression of mature adipocytes isolated from gWAT, ex vivo cultured without or with ONX-0914 (200nM) for 24h under basal, lipolytic (10 µM isoproterenol), and lipogenic (100 nM insulin) conditions. Expressed as mean ± SEM,* ***BI****) 1-way ANOVA with Holm-Sidak posttest,* ***C****) unpaired two tailed t-test,* ***F****) Pearson correlation, *p < 0.05, **p < 0.01, ***p < 0.001, **** p < 0.0001.*

cytometry (Fig. 6A). A single injection of ONX-0914 already led to infiltration of $CD11b^{+}F4/80^{-}$ cells, most likely neutrophils (Fig. 6B). A week of ONX-0914 treatment led to increased overall immune cell counts ($CD45^{+}CD34^{-}$) and accumulation of $CD11b^{+}F4/80^{+}$ monocytes/macrophages (Fig. 6B), confirming the infiltration of immune cells upon ONX-0914 treatment. Furthermore, treatment with ONX-0914 for a week massively reduced the number of adipose stem cells and preadipocytes in gWAT SVF (Fig. 6CD).

To assess in more detail whether ONX-0914 affected the mature adipocyte population and how ONX-0914 caused the innate immune infiltrate in gWAT and reduction in gWAT mass, RNA was isolated from the adipocyte cell fraction after 1 week of treatment with ONX-0914. UCP-1 expression was not increased (Fig. 6E), suggesting that beiging of white adipose tissue due to ONX-0914 treatment did not underlie a reduction in body weight in ONX-0914 treated mice. Surprisingly PPAR-γ expression, a marker for mature adipocytes, was decreased approximately 3-fold with a concomitant increase in CCL-2 and CD68 expression (Fig. 6E), indicating the presence of macrophages in the adipocyte cell fraction. Correlation analysis of CCL2 expression and CD68 of the ONX-0914 treated group, suggests that CCL2 expression was unlikely to be derived from solely macrophages ($r2 = 0.4494$, $p = 0.1451$) (Fig. 6F). Therefore we determined whether mature adipocytes could have been a source of CCL2 expression in the adipocyte fraction of ONX-0914 treated mice. To assess this, mature adipocytes were isolated from gWAT of 40 week old female $ApoE^{-/-}$ animals on chow diet, and we determined whether immunoproteasomal subunits were expressed in mature adipocytes by qPCR. Freshly isolated mature adipocytes did express immunoproteasomal PSMB8 (LMP7), PSMB9 (LMP-2) and PSMB10 (MECL-1) (Fig. 6G), although expression of immunoproteasomal subunits was low compared to expression of proteasomal subunits PSMB5 (β5), PSMB6 (β1) PSMB7 (β2), and expression of immunoproteasomal subunits in splenocytes (Fig. 6H). Exposure of mature adipocytes overnight to ONX-0914 (200 nM) did not reduce the expression of PPAR-γ, but significantly induced CCL-2 expression in insulin and isoproterenol treated adipocytes (Fig. 6I), indicating that ONX-0914 treatment can directly affect mature adipocytes, causing CCL2 induction, which could lead to WAT inflammation.

ONX-0914 reduces intestinal lipid uptake through a macrophage dependent mechanism

To further investigate the mechanism of ONX-0914 mediated reduction of gWAT mass, we assessed whether LMP7 inhibition influenced energy expenditure using metabolic cages. Since TG levels were lowered by LMP7 inhibition we also studied the effect of ONX-0914 on clearance of iv injected VLDL-like particles with radiolabeled [^{14}C]cholesteryl oleate and glycerol tri[^{3}H]oleate *(26)*. Because our initial studies in LDLr deficient mice may have prevented a cholesterol-lowering effect due to the absence of a functional LDLr *(27)*, we

opted to use APOE*3-Leiden.CETP mice in this experiment. After 3 weeks of WTD feeding, ONX-0914 treatment was started for 2.5 weeks (10 mg/kg, 3 times weekly).

Two weeks of treatment of APOE*3-Leiden.CETP mice with ONX-0914 led to reduced body weight gain compared to control treatment (Fig. 7A). Similar to the studies using LDLr KO mice, ONX-0914 reduced fat mass but not lean mass as assessed by EchoMRI (Fig. 7B), while overall food intake throughout the study was similar (Fig. 7C). Unexpectedly, locomotor activity (Fig. 7E) and energy expenditure (Fig. 7F) were decreased during the dark phase after treatment. Carbohydrate oxidation decreased directly after ONX-0914 treatment (Fig. 7G) and was accompanied by increased fat oxidation after treatment (Fig. 7H). The night after treatment (29-41h after treatment) locomotor activity normalized (Fig. 7E) and fat oxidation decreased (Fig. 7G) whilst carbohydrate oxidation tended to increase (Fig. 7H). Because locomotor activity was lowered and fat combustion was increased after treatment, we hypothesized that food intake could be reduced directly after treatment, and was compensated for during the 24h after that. Because this should be reflected in the fecal output, feces was collected the first 18h after treatment and the subsequent 24h. ONX-0914 treatment reduced total fecal weight in the first 18h and increased in the 18h-42h timeframe (Fig. 7D), suggesting that food intake may indeed be inhibited directly upon ONX-0914 treatment. TG and total nonHDL-cholesterol levels were lowered by LMP7 inhibition (Fig. S10A/B). Clearance of [^{14}C]cholesteryl oleate and glycerol tri[^{3}H]oleate levels from iv injected VLDL-like particles was slightly slower in ONX-0914 treated animals (Fig. S10C), indicating that lowered TG and TC levels were not due to a faster uptake from the blood.

Similar to the results in LDLr$^{-/-}$ mice, macrophage accumulation was detected in gWAT, marked by enhanced CD68 gene expression upon ONX-0914 treatment (Fig. S11A). M1 macrophage markers SOCS3, TNF-α, and IL-6, and M2 macrophage markers Arginase-I and IL-10 gene expression were increased to a similar extent upon LMP7 inhibition (Fig. S11A), indicating that the accumulated macrophages were not skewed towards a particular phenotype (Fig. S11B). Unlike in the previous experiments in which we assessed immune infiltrate in gWAT after shorter periods of ONX-0914 treatment, we did not find neutrophil accumulation in gWAT after 2.5 weeks of ONX-0914 treatment (Fig. S11C), and like previous experiments we did not find T cell accumulation in gWAT (Fig. S11C). No accumulation of macrophages was observed in interscapular brown adipose tissue tissue (iBAT) (Fig. S11D/E) or liver (Fig. S11F), suggesting that macrophage accumulation was WAT specific.

Because it was previously reported that intestinal lipid uptake was reduced in LMP7 deficient mice *(28)* we wondered whether lipid uptake was affected in ONX-0914 treated mice, and whether macrophages, consistently found to accumulate in gWAT after ONX-0914 treatment, were involved in this process. To assess involvement of the accumulated

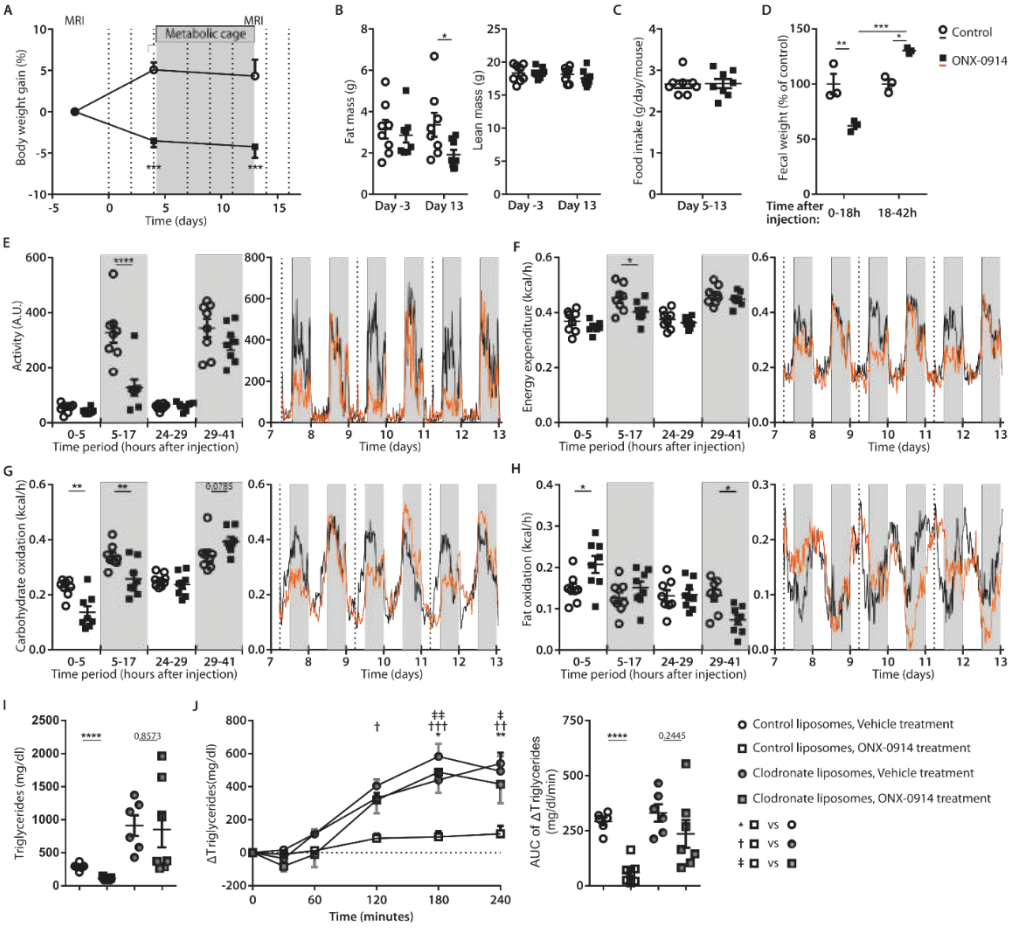

Fig. 7 ONX-0914 mediated weight loss is mediated by reduced intestinal lipid uptake A*) Body weight change over the course of the the metabolic cage study and its experimental setup. Dotted lines indicate control and ONX-0914 injections.* ***B****) At day -3 and 13 body composition was analyzed by EchoMRI. From day 5-13 animals were single housed in metabolic cages in which* ***C****) food intake,* ***E****) activity,* ***F****) energy expenditure and* ***H****) glucose and* ***G****) lipid utilization were determined.* ***D****) Feces was collected from the bedding of group housed animals at day 15 (0-18h after treatment) and day 16 (18-42h after treatment), and weighed.* ***I****) Baseline TG levels in blood plasma, obtained just before oral gavage with olive oil (200 µL).* ***(J)*** *Change in blood plasma TG levels at several timepoints after oral gavage with olive oil (left panel), and area under the curve of the change in TG levels (panel right) . Expressed as mean ± SEM,* ***A,D-H, J****) (left panel) two-way paired ANOVA with Holm-Sidak posttest,* ***B****) (day 13) and* ***C****) two-tailed T-test,* ***I,J****) (right panel) multiple two-tailed T-test with Holm-Sidak posttest, *p < 0.05, **p < 0.01, ***p < 0.001, **** p < 0.0001.*

macrophages, intraperitoneal macrophages were depleted with ip injections of clodronate

liposomes a day prior to control or ONX-0914 treatment and compared to mice injected with empty liposomes. ONX-0914 treatment (10 mg/kg, 4 injections every other day) enhanced macrophage and neutrophil numbers in gWAT like previously after a week of ONX-0914 treatment (Fig. S12A-D). Clodronate liposome treatment successfully reduced $CD11b^{+}F4/80^{+}CD206^{+}$ adipose tissue resident macrophage levels (Fig. S12A/B), and reduced accumulation of $CD206^{-}$ macrophages (Fig. S12A/B) and neutrophils (Fig. S12C/D) after ONX-0914 treatment. After three ONX-0914 injections mice were fasted overnight after which blood was collected, and mice received an oral bolus of 200 µl olive oil after which blood was collected at several time points to assess TG levels. Macrophage depletion increased baseline TG levels (Fig. 7G) in line with previous data *(29)*, whilst only in the control liposome/ONX-0914 treated group triglyceride uptake was decreased (Fig. 7H), suggesting that ONX-0914 acted through a macrophage population to reduce intestinal lipid uptake. In LMP7 deficient animals, reduced intestinal lipid uptake was believed to be the result of a lower expression of fat digesting lipases, pancreatic lipase (Pnlip) and pancreatic lipase-related protein 2-like (Pnliprp2) *(28)*, however we did not observe this (Fig. S13A) nor did we observe reduced expression of proteins involved in intestinal lipid uptake (Fig. S13B).

To further investigate the mechanism through which macrophages are involved in ONX-0914 induced weight loss, we performed a literature search for macrophage derived factors known to temporarily reduce food intake and activity, as seen in our metabolic cage study, and known to reduce body weight. From this literature search, we identified GDF15 which was recently described to induce similar metabolic profile as we observed with LMP7 inhibition *(30)*. GDF15 levels were indeed increased in blood plasma from ONX-0914 treated mice from multiple studies, shown for the initial atherosclerosis study (Fig. S14A). Therefore, we assessed whether induction of GDF15 upon treatment with ONX-0914 was the cause of the reduced body weight and treated $GDF15^{-/-}$ mice with the LMP7 inhibitor. Since already after a week of treatment a strong trend towards weight loss was observed in $GDF15^{-/-}$ mice treated with ONX-0914 (Fig. S14B), it is unlikely that GDF15 mediated ONX-0914-induced weight loss.

Besides reducing atherosclerosis through its immunosuppressive properties, ONX-0914 thus reduces white adipose tissue weight but not lean mass through reduced intestinal lipid uptake, and causes macrophage accumulation in gWAT. Macrophages appear to be involved in ONX-0914 mediated reduction in intestinal lipid uptake, however the exact mechanism in which intestinal lipid uptake is affected by LMP7 inhibition remains to be elucidated.

Discussion

ONX-0914 mediated LMP7 and LMP2 inhibition *(10)* has proven to be effective in reducing disease severity in various auto-immune animal models through immune inhibition, but had not yet been tested in the context of atherosclerosis. In this study we show that ONX-0914 treatment reduced atherosclerosis in female LDLr$^{-/-}$ mice fed a WTD. Unexpectedly LMP7/LMP2 inhibition also reduced body weight by reducing WAT and substantially improved markers of metabolic syndrome.

Atherosclerosis is characterized by lipid accumulation in vessel wall and subsequent chronic immune activation of the vessel wall, aggravating the disease. Oxidation and aggregation of LDL in the subendothelial space promotes uptake of LDL by macrophages and other APCs and results in activation of autoreactive (ox)LDL specific T cells. The inflammatory response in atherosclerosis is marked by a Th1 response *(2, 31)*, resulting in production of the atherogenic Th1 cytokines IFN-γ *(32–36)* and TNFα *(37, 38)*. Because of the detrimental effects of the Th1 response in atherosclerosis *(2, 39, 40)* we aimed to inhibit this response. Inhibition of the immunoproteasomal LMP7 subunit with ONX-0914 was previously described to inhibit Th1 and Th17 development *(9, 11)*, reduce secretion of pro-inflammatory cytokines *(9, 41)*, and reduce various auto-immune diseases in experimental models. Therefore, we were interested to study the effect of ONX-0914 on atherosclerosis.

Treatment with ONX-0914 reduced atherosclerosis in LDLr$^{-/-}$ mice fed WTD for 7 weeks. At this time point we did not observe reductions in Th1 cytokines in serum and in supernatant of αCD3/αCD28 stimulated splenocytes, but did observe an overall decrease in CD4 and CD8 Tem and Tcm cell populations in different lymphoid compartments, confirming the inhibitory effect of LMP7/LMP2 inhibition on T cell function. Circulating effector memory T cells were previously found to correlate with carotid intima-media thickness independent of classical CVD risk factors in human, and were increased in patients with stable angina and acute myocardial infarction compared to controls *(42)*, indicating that is likely that ONX-0914 mediated reduction in circulating effector T cells helped reducing atherosclerosis.

Besides direct inhibition of T cells, ONX-0914 treatment also reduced the cDC content in the spleen and reduced cDC content and activation in mesenteric lymph nodes and cervical lymph nodes which drain the peritoneal cavity and intestines (atherosclerosis unrelated) *(42)* and drain the aorta and supra-aortic arteries (atherosclerosis related) *(43)* respectively, providing an indirect way to inhibit T cell activation. This is in line with the finding that immunoproteasome deficient DCs are inferior at priming T cell responses compared to wild type DCs *(8)*. Enhanced activation of dendritic cells previously proofed to be atherogenic and led to increased CD4 and CD8 T cell activation *(18)*, therefore the reduced DC numbers and activation are likely to have contributed to the smaller lesions observed after ONX-0914

treatment. We found that overnight incubation of bone marrow derived DCs with ONX-0914 reduced DC viability and led to a trend towards reduced BMDC activation, indicating that reduced DC levels and activation in vivo were most likely a direct result of ONX-0914 treatment.

The exact molecular mechanisms by which immune cells are inhibited by proteasomal inhibition are largely unknown, however have been proposed to involve the unfolded protein response (UPR) pathway *(17)* which is activated in response to accumulation of unfolded and misfolded proteins in the ER, inducing ER stress *(44)*. Presumably the primary task of the UPR is regulating the expression of numerous genes aimed to regain homeostasis in the ER or induce apoptosis if ER stress remains unresolved *(44)*. An important secondary task of the UPR in immune cells may also be the inhibition of activation of immune cells which cannot accurately process incoming signals due to accumulation of ubiquitinated proteins, preventing uncontrolled tissue damage. In light of such a protective mechanism, it is fitting that Nrf2 (*n*uclear factor erythroid-derived 2-*r*elated *f*actor *2*), which under normal circumstances is very rapidly degraded by the proteasome but stabilized upon proteasome inhibition *(45)*, upregulates gene expression of proteasomal subunits to regain healthy protein homeostasis *(46)*, and is known to suppress the immune system *(47–53)*.

Next to developing atherosclerosis, LDLr$^{-/-}$ mice on WTD develop obesity, obesity associated metabolic syndrome, and insulin resistance *(54, 55)*. In addition to reducing atherosclerosis, ONX-0914 consistently reduced body weight in WTD fed LDLr$^{-/-}$ mice and APOE*3-Leiden.CETP mice, markedly reducing WAT mass while preserving lean mass, and inducing improved metabolic parameters such as lowered insulin levels, lowered fasting blood glucose, lowered TG levels, and in APOE*3-Leiden.CETP mice, also lowered cholesterol levels. To ensure that weight loss in ONX-0914 treated mice was not caused by (hepato)toxicity, we assessed the activity of liver enzymes ALAT and ASAT in the blood, and Cyp3A11 expression in the liver. ALAT and ASAT activity, and Cyp3A11 expression were not elevated, indicating no toxic side-effects of ONX-0914 treatment. To our knowledge this is the first study to show that LMP7 inhibition using the LMP7 specific inhibitor ONX -0914 has metabolic effects in addition to its immunomodulatory effects, which is likely the consequence of the use of a WTD in our study, leading to the substantial accumulation of WAT mass and development of metabolic syndrome, versus the use of lean mice on chow diet in previous studies applying ONX-0914 *(9–17)*. In addition, disease-related weight loss due to induction of colitis *(12)*, EAE *(11)* or arthritis *(9)*, may have masked the metabolic effects of ONX-0914 in these disease models.

We found that ONX-0914 reduced WAT mass, not through increased energy expenditure or reduced overall food intake, but through reduced intestinal uptake of lipids, similar to

findings in LMP7 deficient animals *(28)*. In the study of Kimura *et al.* reduced intestinal lipid uptake in LMP7 deficient mice was attributed to lowered expression of pancreatic lipases Pnlip and Pnlrp2 *(28)*, however pharmacological inhibition of LMP7/LMP2 did not lead to lowered expression of Pnlip and Pnlrp2 in our study. Indeed, intestinal uptake of lipids is minimally affected in Pnlip *(56)* or Pnlrp2 deficient mice *(57)*. Instead, we found that ONX-0914 initially induced neutrophil infiltration and subsequently macrophage accumulation in gWAT. We found that ONX-0914 mediated inhibition of lipid absorption was peritoneal macrophage dependent, as intestinal lipid uptake was not affected in animals treated with ONX-0914 intraperitoneally administered clodronate liposomes. From a literature search, we found GDF15 as a macrophage derived factor which is known to (temporarily) reduce food intake and induce weight loss *(30)*. ONX-0914 treatment upregulated GDF15 levels in the blood, but as GDF15$^{-/-}$ mice also lost weight when treated with ONX-0914, GDF15 did not appear to mediate ONX-0914 induced weight loss in ONX-0914 treated mice. More research is needed to assess the exact mechanism in which ONX-0914 induces loss of WAT mass. Other macrophage derived products, including IL-1β *(58)* and IL-15 *(59)*, were previously found to reduce intestinal lipid uptake.

Moreover, the innate inflammatory response in gWAT is most likely responsible for the enhanced TNF-α, IL-1β and IL-6 levels in blood upon ONX-0914 treatment. Interestingly, patients with a loss of function mutation in PSMB8, coding for LMP7, present themselves with similar symptoms including elevated serum IL-6 levels, white adipose tissue inflammation, and lipodystrophy *(23)*. These effects of dysfunctional LMP7 were attributed to dependency of preadipocytes on LMP7 for differentiation towards mature adipocytes. Moreover, Psmb8$^{-/-}$ mice have lowered preadipocytes and adipose stem cell numbers *(23, 24)*. In line with these findings, we found that ONX-0914 treatment severely reduced preadipocyte and adipose stem cell numbers in gWAT. Since we found that isolated mature adipocytes express immunoproteasomal catalytic subunits and upregulate CCL2 in response to overnight exposure to ONX-0914, this provides a direct mechanism for ONX-0914 induced innate immune infiltrate in gWAT. Similar to LMP7/LMP2 inhibition in immune cells, ONX-0914 is likely to have affected proteostasis in adipocytes. UPR activation in multiple cell types of non-hematopoietic origin was found to induce CCL2 expression *(60–62)*, which may explain CCL2 expression in adipocytes and gWAT in response to LMP7 inhibition. The presence of macrophages in the buoyant adipocyte fraction after gWAT digestion in the ONX-0914 treated group, indicates either tight interaction between macrophages and adipocytes, or enhanced uptake of lipids by gWAT macrophages through uptake of free fatty acids or efferocytosis of apoptotic adipocytes which could have contributed to the lowered TG levels in blood plasma of ONX-0914 treated mice.

In contrast to our studies with ONX-0914, no immune infiltrate was observed in gWAT from LMP7 deficient mice *(28)*, and no effect of LMP7 deficiency was found on body weight and atherosclerosis in LDLr$^{-/-}$ animals on WTD for 6 weeks and 24 weeks *(63)*. It was argued that in the LMP7/LDLr dKO mice the lowered expression of the immunoproteasome constituents LMP2 and MECL-I was effectively compensated by enhanced constitutive proteasome expression leading to similar overall caspase-like, trypsin like, and chymotrypsin-like proteolytic activities in BMDM cell lysates from LMP7 deficient and sufficient animals *(63)*. In line with the discrepancy between LMP7 deficiency *(63)* and ONX-0914 treatment in our study with respect to atherosclerosis, similar data were observed in experimental autoimmune EAE, where LMP7 deficiency did not affect disease whereas treatment with ONX-0914 did reduce disease severity *(11)*. These data seem to correlate with the recent discovery that ONX-0914 acts through inhibition of not only LMP7, but also through inhibition of LMP2 inhibition, and that inhibition of both subunits was needed to ameliorate experimental colitis and EAE *(10)*.

Treatment of mice with ONX-0914 reduces atherosclerosis and considerably reduces WAT mass in obese mice fed a WTD, concomitantly improving parameters of metabolic syndrome. Because atherosclerosis is still the primary cause of death, and the obesity epidemic is feeding metabolic syndrome related diseases worldwide, immunoproteasomal inhibition could be a valuable therapeutic tool for the western world to combat both. Identification of the mechanisms behind ONX-0914 reduced weight loss could allow more specific treatment options.

Materials and Methods

Animals

All animal work was approved by the Leiden University Animal Ethics Committee and the animal experiments were performed conform the guidelines from Directive 2010/63/EU of the European Parliament on the protection of animals used for scientific purposes. Mice were housed in individual ventilated cages with aspen bedding, in groups of 2–4 mice per cage except for the duration of the metabolic cage measurements, during which mice were single housed. Mice were fed a regular chow diet prior to initiation of the *in vivo* experiments after which LDLr$^{-/-}$ (Jackson Laboratory; original purchase, further bred in house), and GDF15$^{-/-}$ (a generous gift from dr. ing. S. de Jager, University Medical Center Utrecht) were fed a WTD containing 0.25% cholesterol 15% cocoa butter (Special Diet Services, Witham, Essex, UK), and APOE*3-Leiden.CETP mice *(64)* were fed a WTD containing 0.1% cholesterol, 15% cocoa butter, and 1% corn oil (HopeFarms, Woerden, The Netherlands) for indicated durations. In the week prior to initiation of treatment mice were randomized based on age and weight. APOE*3-Leiden.CETP mice were additionally randomized based on lean and fat mass, and TC

and TG levels. Mice were intraperitoneally treated with ONX-0914 *(65)* (synthesized by the Leiden Institute of Chemistry) at a concentration of 10 mg/kg, 3 times weekly for the indicated durations. ONX-0914 was solubilized in DMSO after which it was diluted in PBS (37°C) to prevent precipitation of ONX-0194 (4% DMSO). 4% DMSO in PBS served as control treatment. Macrophages were depleted in the indicated experiment with 110 mg/kg clodronate liposomes or treated with an equivalent amount of empty liposomes (both purchased at clodronateliposomes.org, Vrije University, Netherlands). At the end-point of the studies using $LDLr^{-/-}$ and $GDF15^{-/-}$ mice, mice were anesthetized by subcutaneous injection with a mix of ketamine (100 mg/mL), sedazine (25 mg/mL) and atropine (0.5 mg/mL) and retro-orbitally exsanguinated, and perfused with PBS. Directly after the final blood withdrawal after the kinetic study with radiolabeled VLDL-like particles in APOE*3-Leiden.CETP mice, mice were sacrificed by cervical dislocation and perfused with PBS to remove radiolabels that had not been taken up by organs.

Indirect calorimetry

After 3 days of acclimatization, O_2 consumption, CO_2 production, and food intake were measured for 6 consecutive days in fully automatic metabolic cages (LabMaster System, TSE Systems, Bad Homburg, Germany). Total EE was estimated from the VO_2 and resting energy requirement. Carbohydrate oxidation was calculated using the formula $((4.585*VCO_2)-(3.226*VO_2))*4$, in which the 4 represents the conversion from mass per time unit to kcal per time unit *(66)*. Similarly, fat oxidation was calculated using the formula $((1.695*VO_2)-(1.701*VCO_2))*9$. Physical activity was monitored using infrared sensor frames. Metabolic cage data from the first 5 h directly after injection at 1 PM with ONX-0914 or vehicle ('Day of treatment', light phase) were analyzed and compared to the same 5-h period 24 h later ('Day after treatment', light phase). For calculations of averages during the dark phase (night on 'Day of/after treatment'), 12 h periods of time were used for analysis.

Preparation of VLDL-like TG-rich emulsion particles and clearance assay

VLDL-like TG-rich emulsion particles (80 nm) containing radiolabeled glycerol tri[^{3}H]oleate (TO) and [^{14}C]cholesteryl oleate (CO) were synthesized like previously *(67)*. In brief, emulsion particles were obtained by sonicating a mixture of TO (70 mg), egg yolk phosphatidylcholine (22.7 mg), CO (3.0 mg), lysophosphatidylcholine (2.3 mg), and cholesterol (2.0 mg), containing [^{3}H]TO (100 µCi) and [^{14}C]CO (10 µCi) tracers, at 54°C using a Soniprep 150 (MSE Scientific Instruments, UK) set at 10 µm output. VLDL-like particles were obtained through density gradient ultracentrifugation using a Beckman SW 40 Ti rotor. First, chylomicron-like particles were discarded by removing the top fraction after centrifugation (20,000 r.p.m., 27 min, 20°C), thereafter the remainder was centrifuged (40,000 r.p.m., 27 min, 20 °C) and VLDL-like particles were isolated and stored at 4 °C under argon and used within 5 days.

To study the *in vivo* clearance of cholesteryl oleate and glycerol trioleate, APOE*3-Leiden.CETP mice treated with ONX-0914 or vehicle for 2.5 weeks were fasted for 4 h directly after a final ONX-0914 injection after which a baseline blood sample was drawn, and 200 µL VLDL-like emulsion particles (1.0 mg TG per mouse) were administered iv. Blood samples were obtained 2, 5, 10, and 15 minutes after administration of the emulsion particles by tail bleeding into paraoxon (Sigma)-coated heparinized capillary tubes (Hawksley, Sussex, England). ^{3}H- and ^{14}C -activity was determined in plasma. Total plasma volume was estimated by multiplying body weight (g) with 0.04706 *(26, 68)*. Half-life times were derived from the half-life constant which was calculated using the log values for ^{3}H and ^{14}C measurements for t = 2, 5, and 10 minutes.

Oral TG loading test, plasma lipoprotein analysis

Mice were fasted overnight, after which a baseline blood sample was drawn. Mice received an oral bolus of 200µl olive oil (Bertolli), and blood was drawn 30, 60, 120, 180, and 240 minutes after that. Blood was collected in Microvette CB300 Lithium-Heparin coated capillary tubes (Sarstedt).

TG and TC levels in blood plasma from the oral TG loading test and other experiments were assessed with commercially available kits (Roche). HDL-cholesterol (HDL-C) levels were determined in supernatant from blood plasma of APOE*3-Leiden mice, upon precipitation of ApoB-containing lipoproteins by addition of 20% polyethylene glycol in 200 mM glycine buffer (pH 10) and measurement of TC in the supernatant. The activity of Aspartate Aminotransferase and Alanine Aminotransferase in blood plasma were assessed with activity assay kits (Sigma, MAK055 and MAK052, respectively) according to manufacturer's protocols.

Thymidine incorporation assay

Splenocytes (200,000 cells/well) were stimulated with anti-CD3e (1 µg/mL) and anti-CD28 (0.5 µg/mL) (both from Thermo Fischer) for 72 h and incubated with 0.5 µCi/well ^{3}H-thymidine (Perkin Elmer) for the last 16 h, or remained unstimulated. Cells were thoroughly washed with PBS and thereafter lysed with natriumhydroxide and taken up in Emulsifier-Safe™ (Perkin Elmer). (^{3}H-thymidine incorporation was measured using a liquid scintillation analyzer (Tri-Carb 2900R). Responses are expressed as the mean disintegrations per minute (dpm). The stimulation index (s.i.) was defined by dividing the dpm under activated conditions by the dpm under non-activated conditions per mouse.

gWAT digestion, SVF and primary adipocyte isolation, and primary adipocyte culture

After perfusion with PBS, gonadal white adipose tissue was excised, and minced in DPBS (Lonza) supplemented with 0.5% BSA (Sigma). Thereafter minced adipose tissue was

incubated in DPBS with 10 mM $CaCl_2$, and 4 mg/mL collagenase type II derived from Clostridium Histolyticum (Sigma) at 37°C, while gently agitated in a rotational shaker. Adipose tissue homogenates were passed over a 300-µm mesh (Elko, Fisher Scientific) and thereafter centrifuged at 150 x g for 10 min at RT. Infranatant was removed, saved for assessment of stromal vascular fraction (SVF) cell populations with flow cytometry or discarded, and remaining floating adipocytes were washed twice with DPBS (Gibco) supplemented with 0.5% BSA. Adipocytes were either directly taken up in GTC and stored at -80°C for gene expression analysis, or cultured overnight in DMEM (Lonza) supplemented with 10% FCS (GE Healthcare Life Sciences), 100 U/ml penicillin/streptomycin (GE Healthcare Life Sciences) and 2mM L-glutamine (Thermo fisher Scientific).

Histology

Hearts were transversally cut in half and incubated in OCT medium for 30 minutes. After 30 minutes hearts were fast frozen on dry ice, and stored at -80oC before cryosections (10 µm) of the aortic root were collected on Superfrost Plus™ Adhesion Microscope Slides (ThermoFisher) and analyzed at 70 µm intervals (7 slides/mice). Neutral fats were stained with Oil Red O to determine the average lesion size of five subsequent sections of the aortic root containing 3 valvular leaflets, as a measure of atherosclerotic lesion size. Lesion collagen content was determined with Masson trichrome staining (Sigma-Aldrich) for 3 subsequent sections in 3 sections containing the aortic root valvular leaflets. Corresponding sections were immunohistochemically stained for macrophages with MOMA-2 antibody (Sanbio, 1:1000 dilution). Slides were blocked with 5% milk powder before primary antibody was added for 2h at RT, after which primary antibody was incubated overnight at 4oC. Then slides were incubated with Goat anti-rat Ig alkaline phosphatase (A8438, Sigma-Aldrich) for 1h at RT, after which BCIP/NBT Substrate (DAKO) was used to stain macrophages blue. Blinded histological analysis was performed using a Leica DM-RE microscope and LeicaQwin software (Leica Imaging Systems, Cambridge, UK).

Flow Cytometry

Extracellular staining (ECS) of single cell suspensions was performed in PBS with 2% FCS and αCD16/32 antibody (93, Biolegend) and eBioscience™ Fixable Viability Dye eFluor™ 780 (ThermoFisher) to discriminate between living and dead cells for 30 minutes at 4°C. For intracellular transcription factor staining after ECS, cells were fixed and permeabilized with the FoxP3 transcription factor buffer set (Thermofisher/eBioscience) according to manufacturer's instructions, and incubated with flow cytometry antibodies for 45 minutes at 4°C. Spleen and lymph nodes were mashed over a 70 µm cell strainer (Greiner) to obtain single cell suspensions and red blood cells were lysed with ACK lysis buffer if necessary.

The following antibodies were purchased at BD biosciences: The following antibodies were purchases at BD Biosciences: CD4-PerCP (RM4-5), CD105-PE-CF594 (MJ7/18), CD31-BV421 (Mec13,3), CD45-FITC (30-F11), Ly6G-FITC (1A8); Biolegend: CD11b-eFluor 450 (M1/70), CD11c-FITC (N418), CD4-BV421 (IM7), CD44-FITC (IM7), CD45-Alexa Fluor 700 (30-F11), CD8-BV510 (53-6.7), CD8-APC (53-6.7), CD206-PE/Cy7 (C068C2), CD34-PE/Cy5 (MEC14.7); eBioscience/Thermofisher scientific: CD115-PE (AFS98), CD11c-PE (N418), CD19-Pacific Blue (eBio1D3), CD19-PE/Cy7 (eBio1D3), CD25-APC (PC61.5), CD25-FITC (PC61.5), CD3e-PE/Cy5 (145-2C11), CD34-PB (RAM34), CD44-APC (IM7), CD62L-APC (MEL-14), CD62L-PB (MEL-14), CD8-PE (16-10A1), CD86-PE (GL1), F4/80-APC (BM8), Foxp3-Pacific Blue (FJK-16s), FoxP3-PE (NRRF-30), GATA-3-PE (TWAJ), Ly6C-PE (HK1.4), Ly6C-PerCP/Cy5.5 (HK1.4), NK1.1-APC (PK136), T-bet-PE/Cy7 (eBio4B10), CD11b-eVolve 605 (M1/70), CD161-PE (HP-3G10), CD86-PE/Cy5 (GL1), CD8a-PE/Texas Red (5H10), SCA-1-APC (CT-6A/6E), MHC-II-PerCP/eFluor 710 (M5/114.15.2), MHC-II-eVolve 655 (M5/114.15.2), SCA-1-PE (D7). Compensation measurements were performed using UltraComp eBeads (ThermoFisher) and ArC Amine-Reactive Compensation Beads (ThermoFisher). Cells were measured with a FACSCanto II (BD Biosciences) and a Cytoflex S flow cytometer (Beckman Coulter) and analyzed using FlowJo software (Tree Star, inc.).

Real-time quantitative PCR

RNA was extracted from adipocytes, and mechanically disrupted gWAT, interscapular brown adipose tissue (iBAT), liver, and spleen, using Trizol reagent following manufacturer's instructions (Invitrogen). Thereafter cDNA was generated using RevertAid M-MuLV reverse transcriptase according to manufacturer’s protocol (Thermo Scientific). Quantitative gene expression was measured using Power SYBR Green Master Mix (Thermo Fisher Scientific) on a 7500 Fast Real-Time PCR system (Applied Biosystems). Gene expression was normalized to housekeeping genes ACTB and RPLP0. A list of all primers can be found in the supplementary table (Table S1).

Multiplex ELISA

Inflammatory cytokines in blood plasma, and culture supernatant of splenocytes stimulated overnight with anti-CD3e (1 µg/mL) and anti-CD28 (0.5 µg/mL) were assessed with a T cell differentiation 17-plex Luminex bead-based assay (eBioscience, EPX170-26087-901) according to manufacturer’s instructions. Metabolic syndrome related biomarkers were assessed in blood plasma with a diabetes 8-plex Luminex bead-based assay (BioRad, 171F7001M) following manufacturer’s protocol. Luminex assays were measured on a MAGPIX System (Luminex).

Statistical Analysis

Statistical analysis was performed using Graphpad Prism (version 7.01). Outliers were removed from analysis by the ROUT method (Q = 1%). For statistical comparison of 2 groups an unpaired two-tailed T-test was used. For comparison of more than 2 groups with one variable a one-way ANOVA was used. For statistical comparison of 2 treatment groups with multiple timepoints a two-way repeated measures ANOVA was used. For the comparison of multiple groups defined by two variables, a two-way ANOVA was used. After multiple comparisons, the Holm-Sidak posttest was used to calculate multiplicity adjusted p-values of individual comparisons. Differences between groups were considered statistically significant at $p < 0.05$.

Acknowledgments

None.

Funding

This work was supported by the European Union's Seventh Framework [603131 to J.K.], which was also supported by financial contribution from Academic and SME/industrial partners. We acknowledge the support from the Netherlands CardioVascular Research Initiative: the Dutch Heart Foundation, Dutch Federation of University Medical Centres, the Netherlands Organisation for Health Research and Development, and the Royal Netherlands Academy of Sciences for funding the the GENIUS II project "Generating the best evidence-based pharmaceutical targets and drugs for atherosclerosis" (CVON2017-2020).

Author contributions

JK, devised the main outlines of the project and supervised the project. **GdB** synthesized ONX-0914 under supervision of **BF** and **HO,** and together advised how to handle ONX-0914. The metabolic study in ApoE*3-Leiden mice was designed, executed and analyzed by **AvD** and **PCNR**. **FHS** designed, executed, analyzed the remainder of the experiments, and wrote the manuscript. **ACF**, **IB**, **MK**, **HD**, **JA**, **PJvS** and **GHMvP** helped carrying out most of the experiments and together with **BF**, **HO**, **AvD**, **PCNR**, and **JK**, gave valuable feedback to improve the studies. **BF**, **HO**, **AvD**, **PCNR**, and **JK** commented on the manuscript.

Competing interests

None.

Data and materials availability

All data associated with this study are available in the main text or the supplementary materials**.**

References

1. *GBD 2013 Mortality and Causes of Death Collaborators, Global, regional, and national age–sex specific all-cause and cause-specific mortality for 240 causes of death, 1990–2013: a systematic analysis for the Global Burden of Disease Study 2013, Lancet 385, 117–171 (2015).*

2. *Z. Mallat, S. Taleb, H. Ait-Oufella, A. Tedgui, The role of adaptive T cell immunity in atherosclerosis: Fig. 1., J. Lipid Res. 50, S364–S369 (2009).*

3. *P. M. Ridker, B. M. Everett, T. Thuren, J. G. MacFadyen, W. H. Chang, C. Ballantyne, F. Fonseca, J. Nicolau, W. Koenig, S. D. Anker, J. J. P. Kastelein, J. H. Cornel, P. Pais, D. Pella, J. Genest, R. Cifkova, A. Lorenzatti, T. Forster, Z. Kobalava, L. Vida-Simiti, M. Flather, H. Shimokawa, H. Ogawa, M. Dellborg, P. R. F. Rossi, R. P. T. Troquay, P. Libby, R. J. Glynn, CANTOS Trial Group, Antiinflammatory Therapy with Canakinumab for Atherosclerotic Disease, N. Engl. J. Med. 377, 1119–1131 (2017).*

4. *A. W. Aday, P. M. Ridker, Targeting Residual Inflammatory Risk: A Shifting Paradigm for Atherosclerotic Disease, Front. Cardiovasc. Med. 6, 16 (2019).*

5. *K. Tanaka, The proteasome: overview of structure and functions., Proc. Jpn. Acad. Ser. B. Phys. Biol. Sci. 85, 12–36 (2009).*

6. *P. M. Kloetzel, Generation of major histocompatibility complex class I antigens: functional interplay between proteasomes and TPPII, Nat. Immunol. 5, 661–669 (2004).*

7. *B. J. Van den Eynde, S. Morel, Differential processing of class-I-restricted epitopes by the standard proteasome and the immunoproteasome, Curr. Opin. Immunol. 13, 147–153 (2001).*

8. *D. A. de Verteuil, A. Rouette, M.-P. Hardy, S. Lavallée, A. Trofimov, É. Gaucher, C. Perreault, Immunoproteasomes shape the transcriptome and regulate the function of dendritic cells., J. Immunol. 193, 1121–32 (2014).*

9. *T. Muchamuel, M. Basler, M. A. Aujay, E. Suzuki, K. W. Kalim, C. Lauer, C. Sylvain, E. R. Ring, J. Shields, J. Jiang, P. Shwonek, F. Parlati, S. D. Demo, M. K. Bennett, C. J. Kirk, M. Groettrup, A selective inhibitor of the immunoproteasome subunit LMP7 blocks cytokine production and attenuates progression of experimental arthritis., Nat. Med. 15, 781–7 (2009).*

10. *M. Basler, M. M. Lindstrom, J. J. LaStant, J. M. Bradshaw, T. D. Owens, C. Schmidt, E. Maurits, C. Tsu, H. S. Overkleeft, C. J. Kirk, C. L. Langrish, M. Groettrup, Co-inhibition of immunoproteasome subunits LMP2 and LMP7 is required to block autoimmunity, EMBO Rep. 19, e46512 (2018).*

11. *M. Basler, S. Mundt, T. Muchamuel, C. Moll, J. Jiang, M. Groettrup, C. J. Kirk, Inhibition of the immunoproteasome ameliorates experimental autoimmune encephalomyelitis, EMBO Mol. Med. 6, 226–238 (2014).*

12. *K. W. Kalim, M. Basler, C. J. Kirk, M. Groettrup, Immunoproteasome subunit LMP7 deficiency and inhibition suppresses Th1 and Th17 but enhances regulatory T cell differentiation., J. Immunol. 189, 4182–93 (2012).*

13. *R.-T. Liu, P. Zhang, C.-L. Yang, Y. Pang, M. Zhang, N. Zhang, L.-T. Yue, X.-L. Li, H. Li, R.-S. Duan, ONX-0914, a selective inhibitor of immunoproteasome, ameliorates experimental autoimmune myasthenia gravis by modulating humoral response, J. Neuroimmunol. 311, 71–78 (2017).*

14. *Y. Nagayama, M. Nakahara, M. Shimamura, I. Horie, K. Arima, N. Abiru, Prophylactic and therapeutic efficacies of a selective inhibitor of the immunoproteasome for Hashimoto's thyroiditis, but not for Graves' hyperthyroidism, in mice, Clin. Exp. Immunol. 168, 268–273 (2012).*

15. *H. T. Ichikawa, T. Conley, T. Muchamuel, J. Jiang, S. Lee, T. Owen, J. Barnard, S. Nevarez, B. I. Goldman, C. J. Kirk, R. J. Looney, J. H. Anolik, Beneficial effect of novel proteasome inhibitors in murine lupus via dual inhibition of type i interferon and autoantibody-secreting cells, Arthritis Rheum. 64, 493–503 (2012).*

16. *M. Basler, M. Dajee, C. Moll, M. Groettrup, C. J. Kirk, Prevention of experimental colitis by a selective inhibitor of the immunoproteasome., J. Immunol. 185, 634–41 (2010).*

17. *J. Li, J. Koerner, M. Basler, T. Brunner, C. J. Kirk, M. Groettrup, Immunoproteasome inhibition induces plasma cell apoptosis and preserves kidney allografts by activating the unfolded protein response and suppressing plasma cell survival factors., Kidney Int. 95, 611–623 (2019).*

18. *D. Lievens, K. L. Habets, A.-K. Robertson, Y. Laouar, H. Winkels, T. Rademakers, L. Beckers, E. Wijnands, L. Boon, M. Mosaheb, H. Ait-Oufella, Z. Mallat, R. A. Flavell, M. Rudling, C. J. Binder, N. Gerdes, E. A. L. Biessen, C. Weber, M. J. A. P. Daemen, J. Kuiper, E. Lutgens, Abrogated transforming growth factor beta receptor II (TGFßRII) signalling in dendritic cells promotes immune reactivity of T cells resulting in enhanced atherosclerosis, Eur. Heart J. 34, 3717–3727 (2013).*

19. *A. Hermansson, D. F. J. Ketelhuth, D. Strodthoff, M. Wurm, E. M. Hansson, A. Nicoletti, G. Paulsson-Berne, G. K. Hansson, Inhibition of T cell response to native low-density lipoprotein reduces atherosclerosis, J. Exp. Med. 207, 1081–1093 (2010).*

20. *K. L. L. Habets, G. H. M. van Puijvelde, L. M. van Duivenvoorde, E. J. A. van Wanrooij, P. de Vos, J.-W. C. Tervaert, T. J. C. van Berkel, R. E. M. Toes, J. Kuiper, Vaccination using oxidized low-density lipoprotein-pulsed dendritic cells reduces atherosclerosis in LDL receptor-deficient mice., Cardiovasc. Res. 85, 622–30 (2010).*

21. *T. Rademakers, E. P. C. van der Vorst, I. T. M. N. Daissormont, J. J. T. Otten, K. Theodorou, T. L. Theelen, M. Gijbels, A. Anisimov, H. Nurmi, J. H. N. Lindeman, A. Schober, S. Heeneman, K. Alitalo, E. A. L. Biessen, Adventitial lymphatic capillary expansion impacts on plaque T cell accumulation in atherosclerosis, Sci. Rep. 7, 45263 (2017).*

22. *C. Schmidt, T. Berger, M. Groettrup, M. Basler, Immunoproteasome Inhibition Impairs T and B Cell Activation by Restraining ERK Signaling and Proteostasis., Front. Immunol. 9, 2386 (2018).*

23. *A. Kitamura, Y. Maekawa, H. Uehara, K. Izumi, I. Kawachi, M. Nishizawa, Y. Toyoshima, H. Takahashi, D. M. Standley, K. Tanaka, J. Hamazaki, S. Murata, K. Obara, I. Toyoshima, K. Yasutomo, A mutation in the immunoproteasome subunit PSMB8 causes autoinflammation and lipodystrophy in humans., J. Clin. Invest. 121, 4150–60 (2011).*

24. *H. Arimochi, Y. Sasaki, A. Kitamura, K. Yasutomo, Differentiation of preadipocytes and mature adipocytes requires PSMB8, 6 (2016), doi:10.1038/srep26791.*

25. *L. van Beek, J. B. van Klinken, A. C. M. Pronk, A. D. van Dam, E. Dirven, P. C. N. Rensen, F. Koning, K. Willems van Dijk, V. van Harmelen, The limited storage capacity of gonadal adipose tissue directs the development of metabolic disorders in male C57Bl/6J mice., Diabetologia 58, 1601–9 (2015).*

26. *M. C. Jong, P. C. Rensen, V. E. Dahlmans, H. van der Boom, T. J. van Berkel, L. M. Havekes, Apolipoprotein C-III deficiency accelerates triglyceride hydrolysis by lipoprotein lipase in wild-type and apoE knockout mice., J. Lipid Res. 42, 1578–85 (2001).*

27. *J. F. P. Berbée, M. R. Boon, P. P. S. J. Khedoe, A. Bartelt, C. Schlein, A. Worthmann, S. Kooijman, G. Hoeke, I. M. Mol, C. John, C. Jung, N. Vazirpanah, L. P. J. Brouwers, P. L. S. M. Gordts, J. D. Esko, P. S. Hiemstra, L. M. Havekes, L. Scheja, J. Heeren, P. C. N. Rensen, Brown fat activation reduces hypercholesterolaemia and protects from atherosclerosis development, Nat. Commun. 6, 6356 (2015).*

28. *H. Kimura, F. Usui, T. Karasawa, A. Kawashima, K. Shirasuna, Y. Inoue, T. Komada, M. Kobayashi, Y. Mizushina, T. Kasahara, K. Suzuki, Y. Iwasaki, T. Yada, P. Caturegli, M. Takahashi, Immunoproteasome subunit LMP7 Deficiency Improves Obesity and Metabolic Disorders., Sci. Rep. 5, 15883 (2015).*

29. *A. Kosteli, E. Sugaru, G. Haemmerle, J. F. Martin, J. Lei, R. Zechner, A. W. Ferrante, Jr., Weight loss and lipolysis promote a dynamic immune response in murine adipose tissue., J. Clin. Invest. 120, 3466–79 (2010).*

30. *S. E. Mullican, X. Lin-Schmidt, C.-N. Chin, J. A. Chavez, J. L. Furman, A. A. Armstrong, S. C. Beck, V. J. South, T. Q. Dinh, T. D. Cash-Mason, C. R. Cavanaugh, S. Nelson, C. Huang, M. J. Hunter, S. M. Rangwala, GFRAL is the receptor for GDF15 and the ligand promotes weight loss in mice and nonhuman primates, Nat. Med. 23, 1150–1157 (2017).*

31. *A. Tedgui, Z. Mallat, Cytokines in Atherosclerosis: Pathogenic and Regulatory Pathways, Physiol. Rev. 86, 515–581 (2006).*

32. *S. C. Whitman, P. Ravisankar, H. Elam, A. Daugherty, Exogenous interferon-gamma enhances atherosclerosis in apolipoprotein E-/- mice., Am. J. Pathol. 157, 1819–24 (2000).*

33. *S. Gupta, A. M. Pablo, X. c Jiang, N. Wang, A. R. Tall, C. Schindler, IFN-gamma potentiates atherosclerosis in ApoE knock-out mice., J. Clin. Invest. 99, 2752–61 (1997).*

34. *I. Voloshyna, M. J. Littlefield, A. B. Reiss, Atherosclerosis and interferon-γ: new insights and therapeutic targets., Trends Cardiovasc. Med. 24, 45–51 (2014).*

35. *R. J. Aiello, P. A. Bourassa, S. Lindsey, W. Weng, E. Natoli, B. J. Rollins, P. M. Milos, Monocyte chemoattractant protein-1 accelerates atherosclerosis in apolipoprotein E-deficient mice., Arterioscler. Thromb. Vasc. Biol. 19, 1518–25 (1999).*

36. *Z. H. Zhou, P. Chaturvedi, Y. L. Han, S. Aras, Y. S. Li, P. E. Kolattukudy, D. Ping, J. M. Boss, R. M. Ransohoff, IFN-gamma induction of the human monocyte chemoattractant protein (hMCP)-1 gene in astrocytoma cells: functional interaction between an IFN-gamma-activated site and a GC-rich element., J. Immunol. 160, 3908–16 (1998).*

37. *N. Bergh, E. Ulfhammer, K. Glise, S. Jern, L. Karlsson, Influence of TNF-α and biomechanical stress on endothelial anti- and prothrombotic genes, Biochem. Biophys. Res. Commun. 385, 314–318 (2009).*

38. *S. Choi, M. Park, J. Kim, W. Park, S. Kim, D.-K. Lee, J. Y. Hwang, J. Choe, M.-H. Won, S. Ryoo, K.-S. Ha, Y.-G. Kwon, Y.-M. Kim, TNF-α elicits phenotypic and functional alterations of vascular smooth muscle cells by miR-155-5p–dependent down-regulation of cGMP-dependent kinase 1, J. Biol. Chem. 293, 14812–14822 (2018).*

39. *E. Laurat, B. Poirier, E. Tupin, G. Caligiuri, G. K. Hansson, J. Bariéty, A. Nicoletti, In vivo downregulation of T helper cell 1 immune responses reduces atherogenesis in apolipoprotein E-knockout mice., Circulation 104, 197–202 (2001).*

40. *A. D. Hauer, C. Uyttenhove, P. de Vos, V. Stroobant, J. C. Renauld, T. J. C. van Berkel, J. van Snick, J. Kuiper, Blockade of Interleukin-12 Function by Protein Vaccination Attenuates Atherosclerosis, Circulation 112, 1054–1062 (2005).*

41. *C. E. Rockwell, J. J. Monaco, N. Qureshi, A Critical Role for the Inducible Proteasomal Subunits LMP7 and MECL1 in Cytokine Production by Activated Murine Splenocytes, Pharmacology 89, 117–126 (2012).*

42. *E. Ammirati, D. Cianflone, V. Vecchio, M. Banfi, A. C. Vermi, M. De Metrio, L. Grigore, F. Pellegatta, A. Pirillo, K. Garlaschelli, A. A. Manfredi, A. L. Catapano, A. Maseri, A. G. Palini, G. D. Norata, Effector Memory T cells Are Associated With Atherosclerosis in Humans and Animal Models, J. Am. Heart Assoc. 1, 27–41 (2012).*

43. *D. Wolf, K. Ley, Immunity and Inflammation in Atherosclerosis, Circ. Res. 124, 315–327 (2019).*

44. *C. Hetz, E. Chevet, S. A. Oakes, Proteostasis control by the unfolded protein response, Nat. Cell Biol. 17, 829–838 (2015).*

45. *D. Stewart, E. Killeen, R. Naquin, S. Alam, J. Alam, Degradation of transcription factor Nrf2 via the ubiquitin-proteasome pathway and stabilization by cadmium., J. Biol. Chem. 278, 2396–402 (2003).*

46. *J. Jang, Y. Wang, H.-S. Kim, M. A. Lalli, K. S. Kosik, Nrf2, a Regulator of the Proteasome, Controls Self-Renewal and Pluripotency in Human Embryonic Stem Cells, Stem Cells 32, 2616–2625 (2014).*

47. *N. M. Reddy, S. R. Kleeberger, T. W. Kensler, M. Yamamoto, P. M. Hassoun, S. P. Reddy, Disruption*

of Nrf2 Impairs the Resolution of Hyperoxia-Induced Acute Lung Injury and Inflammation in Mice, J. Immunol. 182, 7264–7271 (2009).

***48**. Y. Ishii, K. Itoh, Y. Morishima, T. Kimura, T. Kiwamoto, T. Iizuka, A. E. Hegab, T. Hosoya, A. Nomura, T. Sakamoto, M. Yamamoto, K. Sekizawa, Transcription factor Nrf2 plays a pivotal role in protection against elastase-induced pulmonary inflammation and emphysema., J. Immunol. 175, 6968–75 (2005).*

***49**. T. Rangasamy, J. Guo, W. A. Mitzner, J. Roman, A. Singh, A. D. Fryer, M. Yamamoto, T. W. Kensler, R. M. Tuder, S. N. Georas, S. Biswal, Disruption of Nrf2 enhances susceptibility to severe airway inflammation and asthma in mice., J. Exp. Med. 202, 47–59 (2005).*

***50**. W. O. Osburn, M. S. Yates, P. D. Dolan, S. Chen, K. T. Liby, M. B. Sporn, K. Taguchi, M. Yamamoto, T. W. Kensler, Genetic or Pharmacologic Amplification of Nrf2 Signaling Inhibits Acute Inflammatory Liver Injury in Mice, Toxicol. Sci. 104, 218–227 (2008).*

***51**. N. G. Innamorato, A. I. Rojo, A. J. García-Yagüe, M. Yamamoto, M. L. de Ceballos, A. Cuadrado, The transcription factor Nrf2 is a therapeutic target against brain inflammation., J. Immunol. 181, 680–9 (2008).*

***52**. D. A. Johnson, S. Amirahmadi, C. Ward, Z. Fabry, J. A. Johnson, The Absence of the Pro-antioxidant Transcription Factor Nrf2 Exacerbates Experimental Autoimmune Encephalomyelitis, Toxicol. Sci. 114, 237–246 (2010).*

***53**. R. K. Thimmulappa, H. Lee, T. Rangasamy, S. P. Reddy, M. Yamamoto, T. W. Kensler, S. Biswal, Nrf2 is a critical regulator of the innate immune response and survival during experimental sepsis, J. Clin. Invest. 116, 984–995 (2006).*

***54**. S. Merat, F. Casanada, M. Sutphin, W. Palinski, P. D. Reaven, Western-Type Diets Induce Insulin Resistance and Hyperinsulinemia in LDL Receptor-Deficient Mice But Do Not Increase Aortic Atherosclerosis Compared With Normoinsulinemic Mice in Which Similar Plasma Cholesterol Levels Are Achieved by a Fructose-Rich Diet, Arterioscler. Thromb. Vasc. Biol. 19, 1223–1230 (1999).*

***55**. S. A. Schreyer, C. Vick, T. C. Lystig, P. Mystkowski, R. C. LeBoeuf, LDL receptor but not apolipoprotein E deficiency increases diet-induced obesity and diabetes in mice, Am. J. Physiol. Metab. 282, E207–E214 (2002).*

***56**. D. Gilham, E. D. Labonté, J. C. Rojas, R. J. Jandacek, P. N. Howles, D. Y. Hui, Carboxyl ester lipase deficiency exacerbates dietary lipid absorption abnormalities and resistance to diet-induced obesity in pancreatic triglyceride lipase knockout mice., J. Biol. Chem. 282, 24642–9 (2007).*

***57**. M. E. Lowe, M. H. Kaplan, L. Jackson-Grusby, D. D'Agostino, M. J. Grusby, Decreased neonatal dietary fat absorption and T cell cytotoxicity in pancreatic lipase-related protein 2-deficient mice., J. Biol. Chem. 273, 31215–21 (1998).*

***58**. J. M. Argilés, F. J. Lopez-Soriano, R. D. Evans, D. H. Williamson, Interleukin-1 and lipid metabolism in the rat., Biochem. J. 259, 673–8 (1989).*

***59**. V. Almendro, N. Carbó, S. Busquets, J. López-Soriano, M. Figueras, E. Ametller, J. M. Argilés, F. J. López-Soriano, Interleukin-15 decreases lipid intestinal absorption., Int. J. Mol. Med. 15, 963–7 (2005).*

***60**. M. Oñate, A. Catenaccio, G. Martínez, D. Armentano, G. Parsons, B. Kerr, C. Hetz, F. A. Court, Activation of the unfolded protein response promotes axonal regeneration after peripheral nerve injury, Sci. Rep. 6, 21709 (2016).*

***61**. L. N. Guthrie, K. Abiraman, E. S. Plyler, N. T. Sprenkle, S. A. Gibson, B. C. McFarland, R. Rajbhandari, A. L. Rowse, E. N. Benveniste, G. P. Meares, Attenuation of PKR-like ER Kinase (PERK) Signaling Selectively Controls Endoplasmic Reticulum Stress-induced Inflammation Without Compromising Immunological Responses., J. Biol. Chem. 291, 15830–40 (2016).*

***62**. S. Zhu, H. Liu, H. Sha, L. Qi, D.-S. Gao, W. Zhang, PERK and XBP1 differentially regulate CXCL10 and*

CCL2 production., Exp. Eye Res. 155, 1–14 (2017).

***63**. B. Hewing, A. Ludwig, C. Dan, M. Pötzsch, C. Hannemann, A. Petry, D. Lauer, A. Görlach, E. Kaschina, D. N. Müller, G. Baumann, V. Stangl, K. Stangl, N. Wilck, Immunoproteasome subunit ß5i/LMP7-deficiency in atherosclerosis, Sci. Rep. 7, 13342 (2017).*

***64**. M. Westerterp, C. C. van der Hoogt, W. de Haan, E. H. Offerman, G. M. Dallinga-Thie, J. W. Jukema, L. M. Havekes, P. C. N. Rensen, Cholesteryl Ester Transfer Protein Decreases High-Density Lipoprotein and Severely Aggravates Atherosclerosis in APOE*3-Leiden Mice, Arterioscler. Thromb. Vasc. Biol. 26, 2552–2559 (2006).*

***65**. K. D. Shenk, F. Parlati, H.-J. Zhou, C. Sylvain, M. Smyth, M. K. Bennett, G. Laidig, Compounds for enzyme inhibition (2008) (available at https://patents.google.com/patent/US20070293465A1/en?oq=2007%2F0293465).*

***66**. F. Péronnet, D. Massicotte, Table of nonprotein respiratory quotient: an update., Can. J. Sport Sci. 16, 23–9 (1991).*

***67**. P. C. Rensen, M. C. van Dijk, E. C. Havenaar, M. K. Bijsterbosch, J. K. Kruijt, T. J. van Berkel, Selective liver targeting of antivirals by recombinant chylomicrons--a new therapeutic approach to hepatitis B., Nat. Med. 1, 221–5 (1995).*

***68**. P. C. Rensen, N. Herijgers, M. H. Netscher, S. C. Meskers, M. van Eck, T. J. van Berkel, Particle size determines the specificity of apolipoprotein E-containing triglyceride-rich emulsions for the LDL receptor versus hepatic remnant receptor in vivo., J. Lipid Res. 38, 1070–84 (1997).*

Supplementary figures

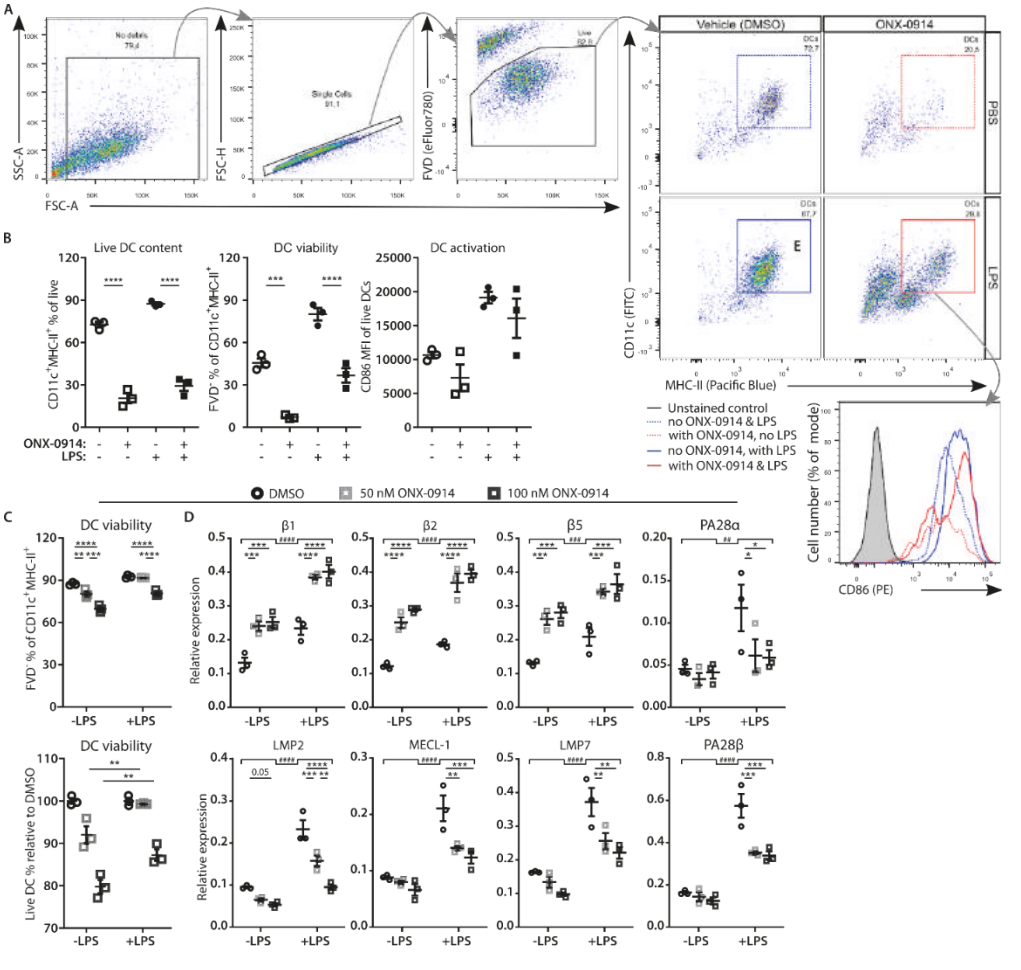

Supplementary Fig. S1 ***LMP7 inhibition directly inhibits DC activation and causes upregulation of constitutive proteasomal active subunits. A****) Bone marrow derived DCs were incubated with ONX-0914 (0-200 nM) overnight in absence or presence of LPS (100 ng/ml) and assessed by flow cytometry.* ***B****) Cell culture viability was assessed by gating as shown in '****A****'. For quantification of DC viability single cells were gated like in '****A****', but directly thereafter CD11c⁺MHC-II⁺ cells were gated after which live DCs were gated. CD86 median fluorescent intensity of the live MHC-II⁺CD11c⁺ population was assessed as a measure for DC activation.* ***C****) Bone marrow derived DCs were incubated with ONX-0914 (0-100 nM) overnight in absence or presence of LPS (100 ng/ml) after which DC viability was determined by flow cytometry like explained in '****B****', and* ***D****) expression of catalytic constitutive and immuno- proteasomal subunits, and immunoproteasomal activators were determined by qPCR. Expressed as mean ± SEM, two-way ANOVA (#) with Holm-Sidak posttest, *p < 0.05, **p < 0.01, *** p < 0.001 **** p < 0.0001.*

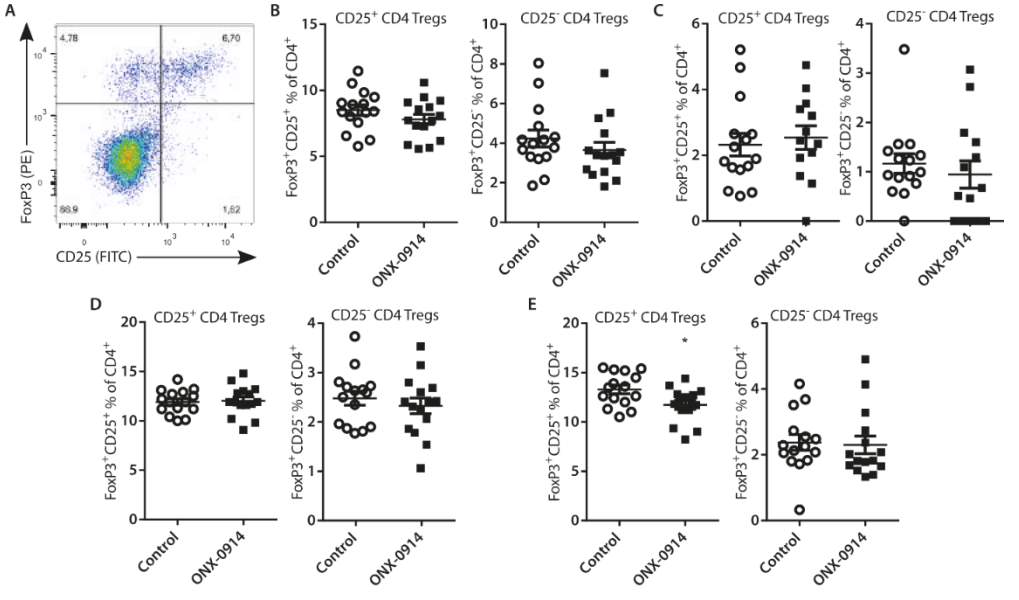

Supplementary Fig. S2 ***Tregs are not increased by ONX-0914 treatment in early atherosclerosis. A****) After sacrifice CD4 T cell FoxP3⁺CD25⁺ and FoxP3⁺CD25⁻populations were determined with flow cytometry, gating shown for the CD4 T cell population in the spleen. Quantification of CD4 Treg populations in* ***B****) spleen,* ***C****) blood,* ***D****) cervical lymph nodes, and* ***E****) mesenteric lymph nodes. Expressed as mean ± SEM, unpaired two tailed t-test, *p < 0.05.*

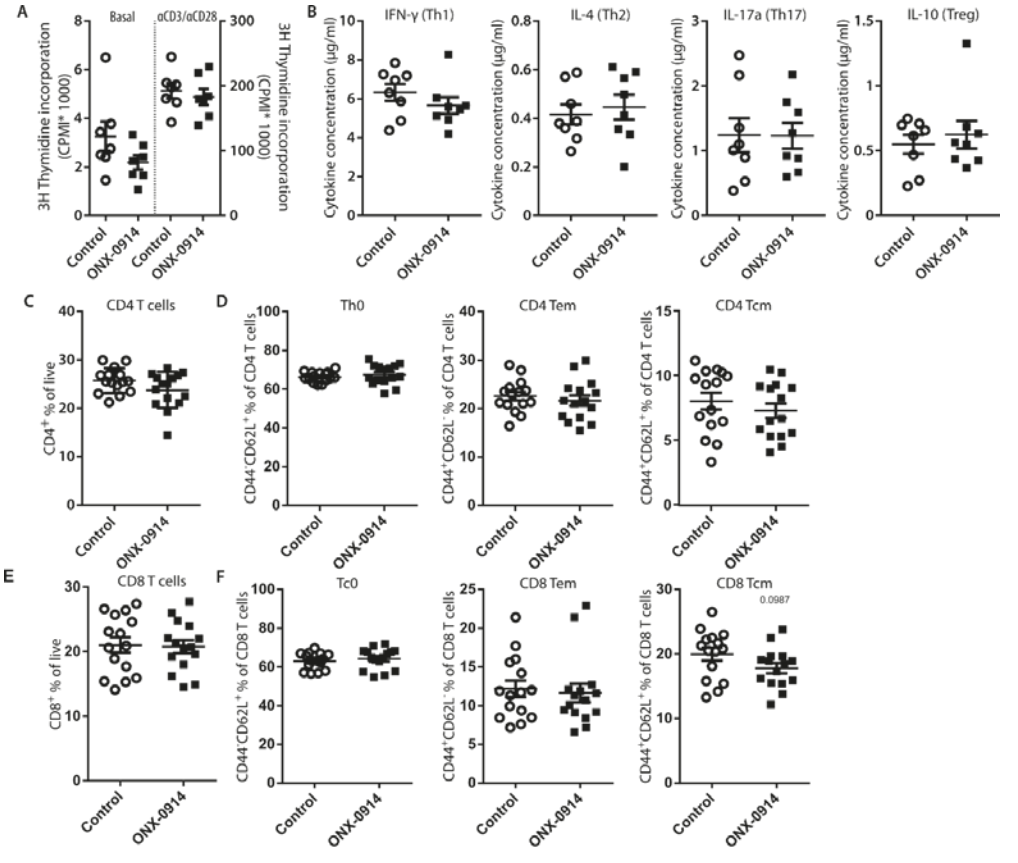

Supplementary Fig. S3 ***LMP7 inhibition does not impact splenic T cell differentiation in early atherosclerosis.*** *(**A**) T cell proliferation in unstimulated or αCD3/αCD28 splenocyte cultures as measured by thymidine incorporation. **B**) Cytokine levels in supernatant of overnight αCD3/αCD28 stimulated splenocyte cultures. C) Overall CD4 T cell levels, **D**) CD4 Tem, Tcm and Th0 levels, and (**C**) overall CD8 T cell levels, and **D**) CD8 Tem, Tcm and Tc0 levels, as determined by flow cytometry. Expressed as mean ± SEM, unpaired two tailed t-test, ***p < 0.001.*

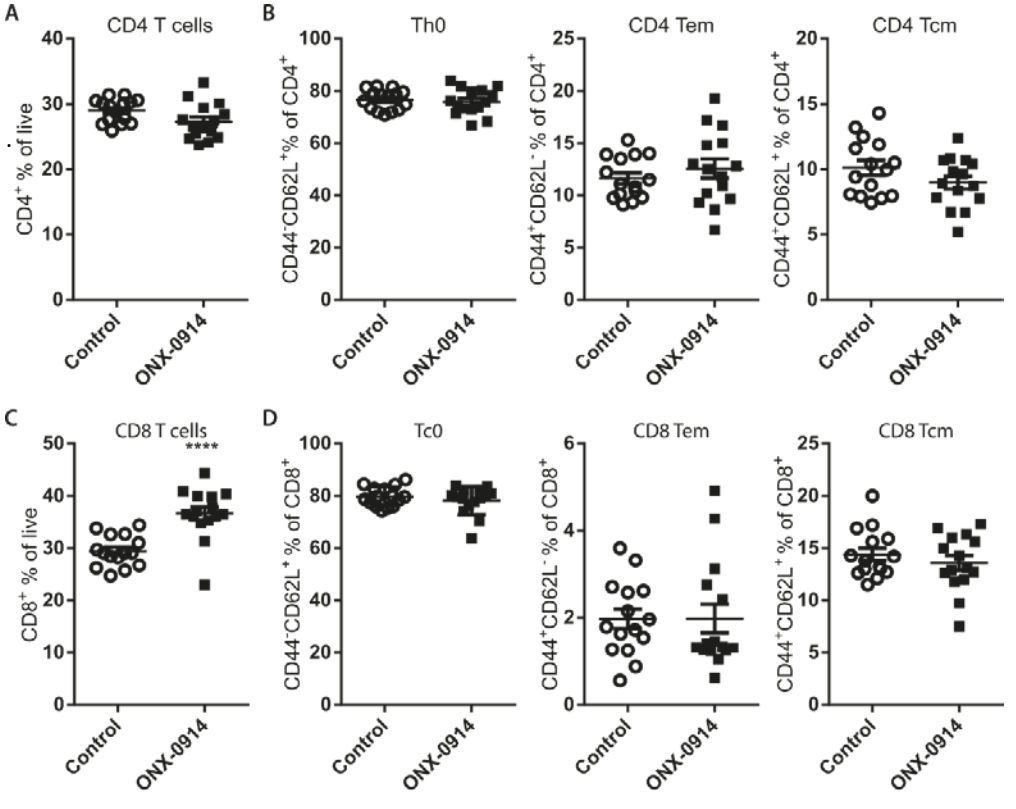

Supplementary Fig. S4 ***Memory and naïve T cell effector populations in cervical lymph nodes.*** *Quantification of flow cytometric analysis of* ***A****) CD4 T cell content and* ***B****) memory and naïve CD4 T cell populations, (****C****) CD8 T cells and* ***D****) memory and naïve CD8 T cell populations in CLN. Expressed as mean ± SEM, unpaired two tailed t-test, ****p < 0.0001.*

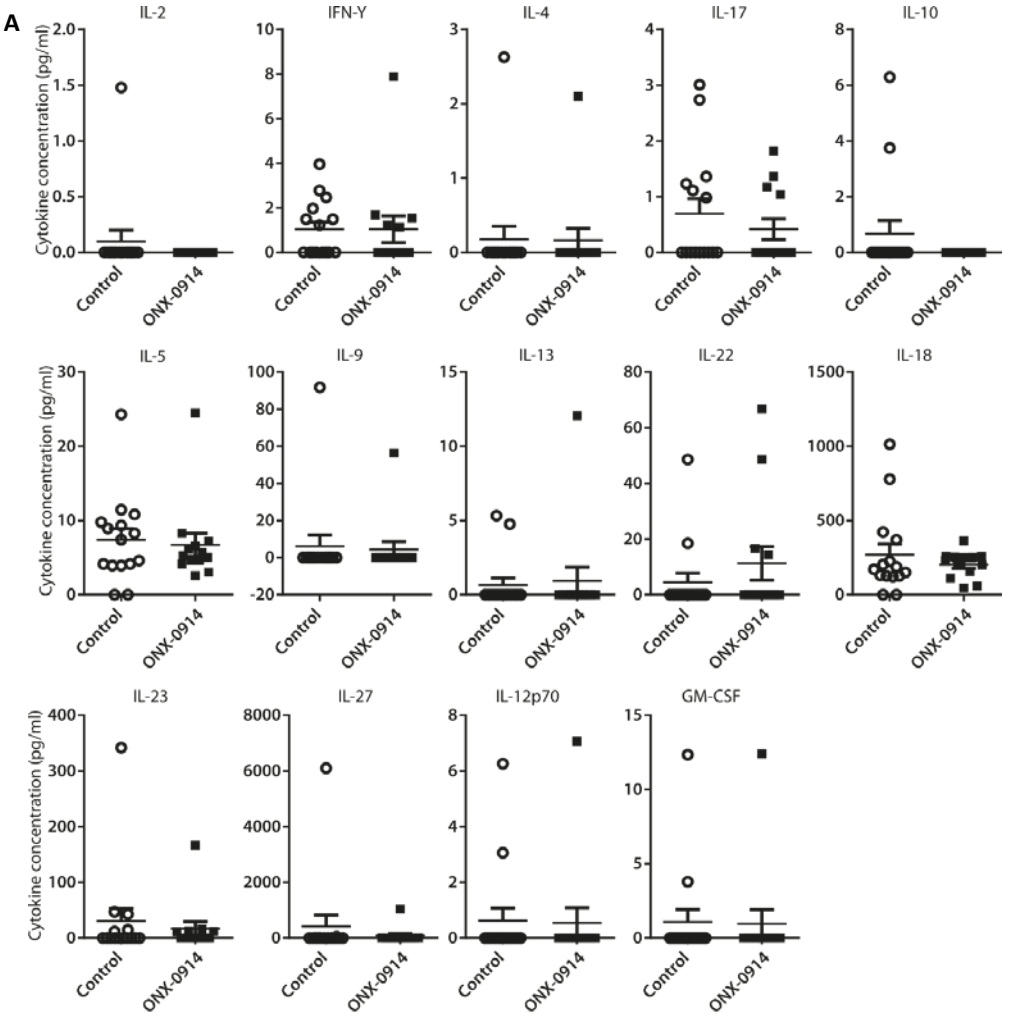

Supplementary Fig. S5 ***Cytokine levels not significantly altered by ONX-0914 treatment.*** ***A****) Quantification of remaining cytokine levels in blood plasma, measured with multiplex ELISA.*

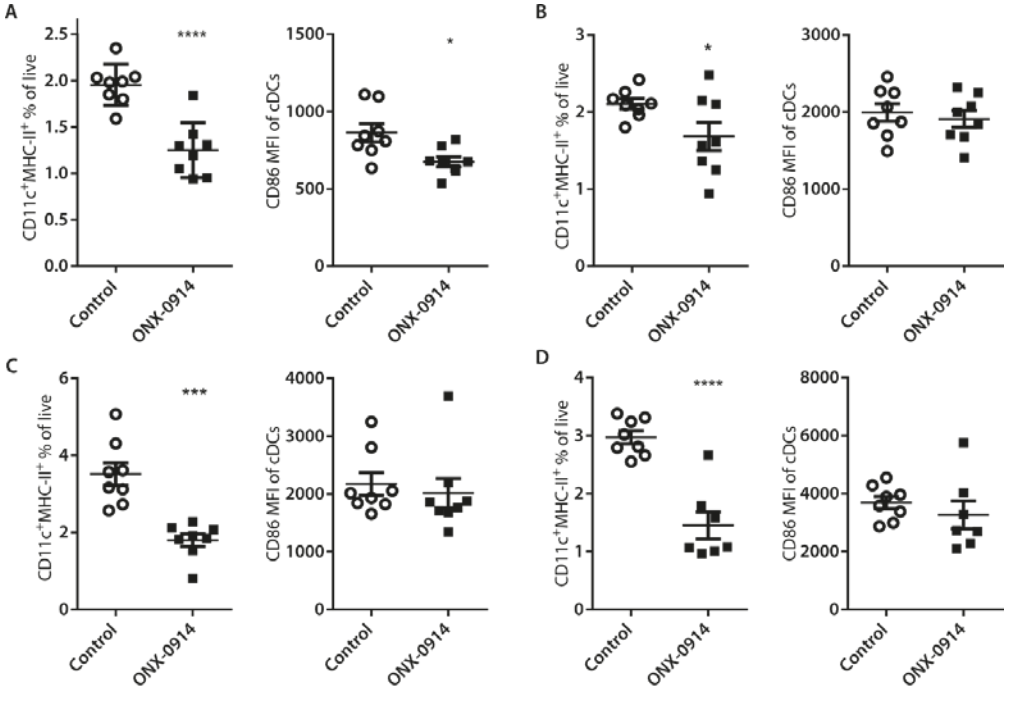

Supplementary Fig. S6 ***Conventional DC levels are reduced by ONX-0914 treatment.*** *Conventional DCs were gated by selection of CD11c⁺MHC-II⁺ cells whilst activation of cDCs was assessed through expression of CD86, as determined by flow cytometric analysis of cells from* ***A****) spleen,* ***B****) cervical lymph nodes,* ***C****) mediastinal lymph nodes, and* ***D****) mesenteric lymph nodes. Expressed as mean ± SEM, unpaired two tailed t-test, *p < 0.05, ***p < 0.001, **** p < 0.0001.*

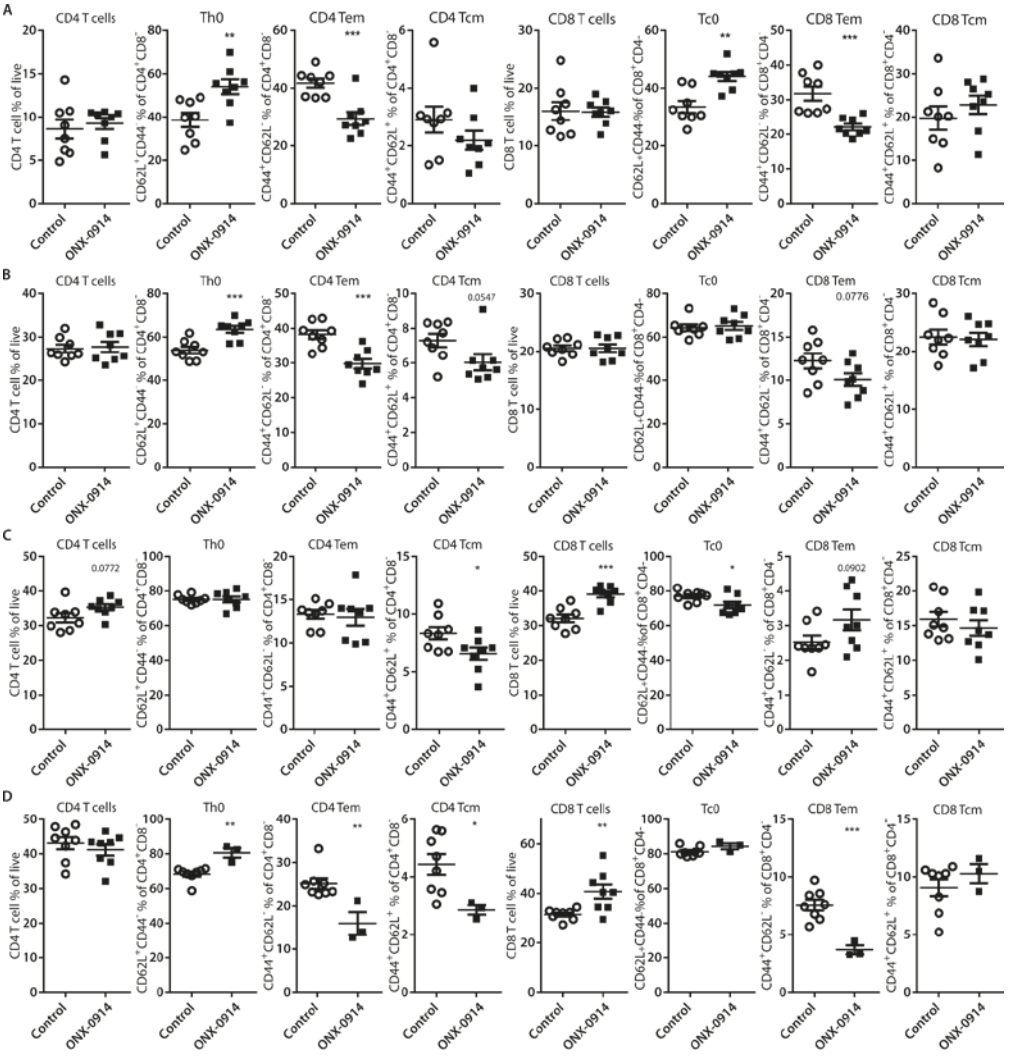

Supplementary Fig. S7 ***ONX-0914 treatment reduces memory T cell levels in various immune compartments.*** *CD4 and CD8 T cells were gated based on expression of CD4 and CD8 respectively. Thereafter, naïve and memory populations were gated based on expression of CD62L and CD44 (Naïve T cells, $CD62L^{+}CD44^{-}$; Effector Memory T cells, $CD44^{+}CD62L^{-}$; Central Memory T cells ($CD44^{+}CD62L^{+}$). Quantification of CD4 and CD8 T cell populations in* ***A****) blood,* ***B****) spleen,* ***C****) cervical lymph nodes, and* ***D****) mesenteric lymph nodes. Expressed as mean ± SEM, unpaired two tailed t-test, *p < 0.05, **p < 0.01, ***p < 0.001.*

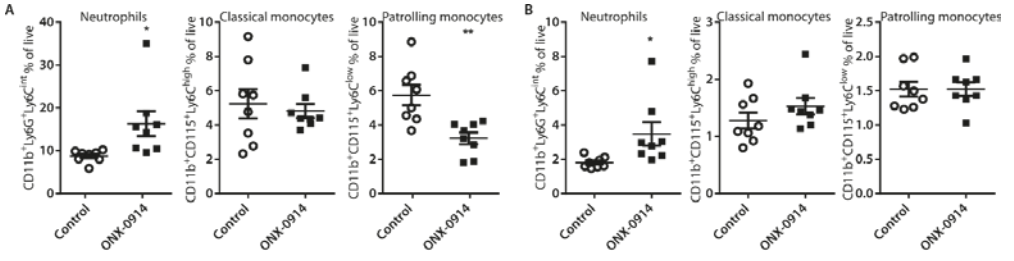

Supplementary Fig. S8 ***ONX-0914 increases neutrophil levels in blood and spleen.*** *Quantification of flow cytometric analysis of neutrophils, classical monocytes and patrolling monocytes in* ***A****) blood and* ***B****) spleen. Expressed as mean ± SEM, unpaired two tailed t-test, *p < 0.05, **p < 0.01.*

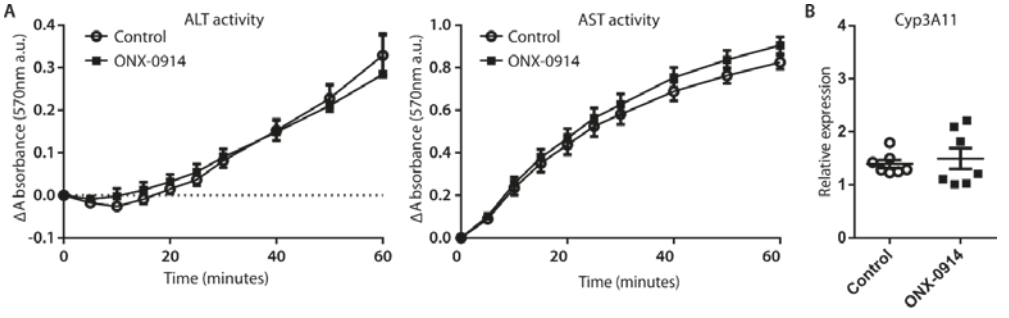

Supplementary Fig. S9 ***Treatment with ONX-0914 does not lead to hepatotoxicity. A****) ALT and AST activity were assessed on blood plasma derived from blood collected at sacrifice after 7 weeks of control or ONX-0914 treatment.* ***B****) Hepatic Cyp3A11 expression. Expressed as mean ± SEM,* ***A****) 2-way repeated measures ANOVA with Holm-Sidak posttest,* ***B****) two tailed t-test, no significant differences.*

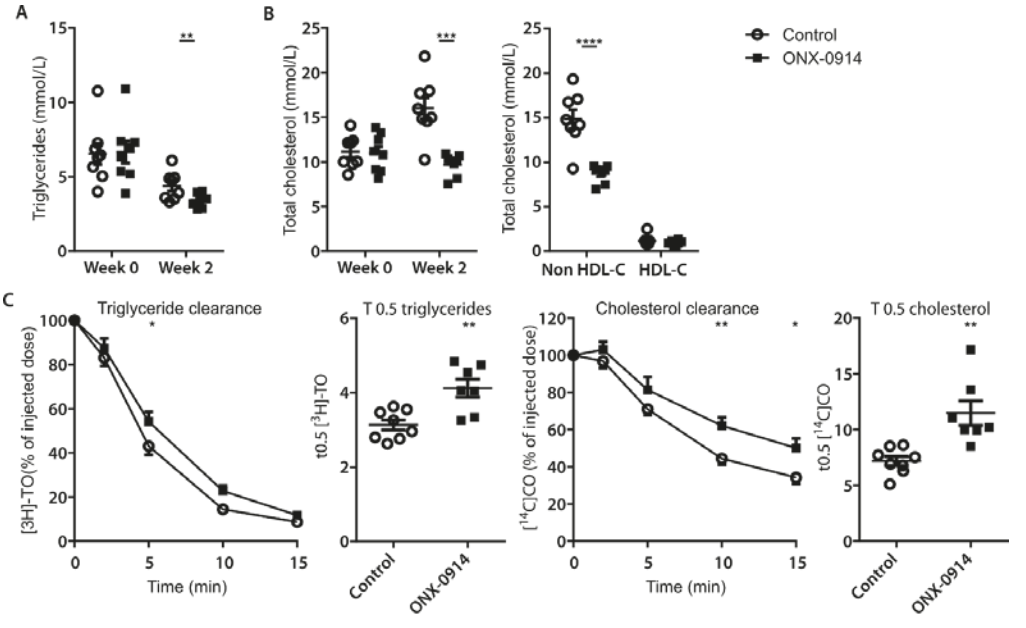

Supplementary Fig. S10 ***TG and TC clearance from the blood is not enhanced by ONX-0914 treatment.*** *After 2.5 weeks of treatment, APOE*3-Leiden.CETP mice received a final control or ONX-0914 injection and were fasted for 4h.* ***A****) Plasma triglyceride levels and* ***B****) cholesterol levels in plasma after 4h starvation.* ***C****) To determine clearance of TG and TC from the blood, VLDL like particles containing radiolabeled [^{14}C]cholesteryl oleate and glycerol tri[^{3}H]oleate were iv administered. Radioactivity in plasma was assessed in blood drawn at indicated time points after VLDL like particle administration, and half life time was approximated. Expressed as mean ± SEM* ***A,B)*** *(left panel),* ***C*** *(1st and 3rd panel from the right), two tailed T-test,* ***B)*** *(right panel) One-way ANOVA Holm-Sidak posttest,* ***C)*** *(1st and 3rd panel from the left) two way ANOVA with Holm-Sidak posttest, *p < 0.05, **p < 0.01, ***p < 0.001, ****p < 0.0001*

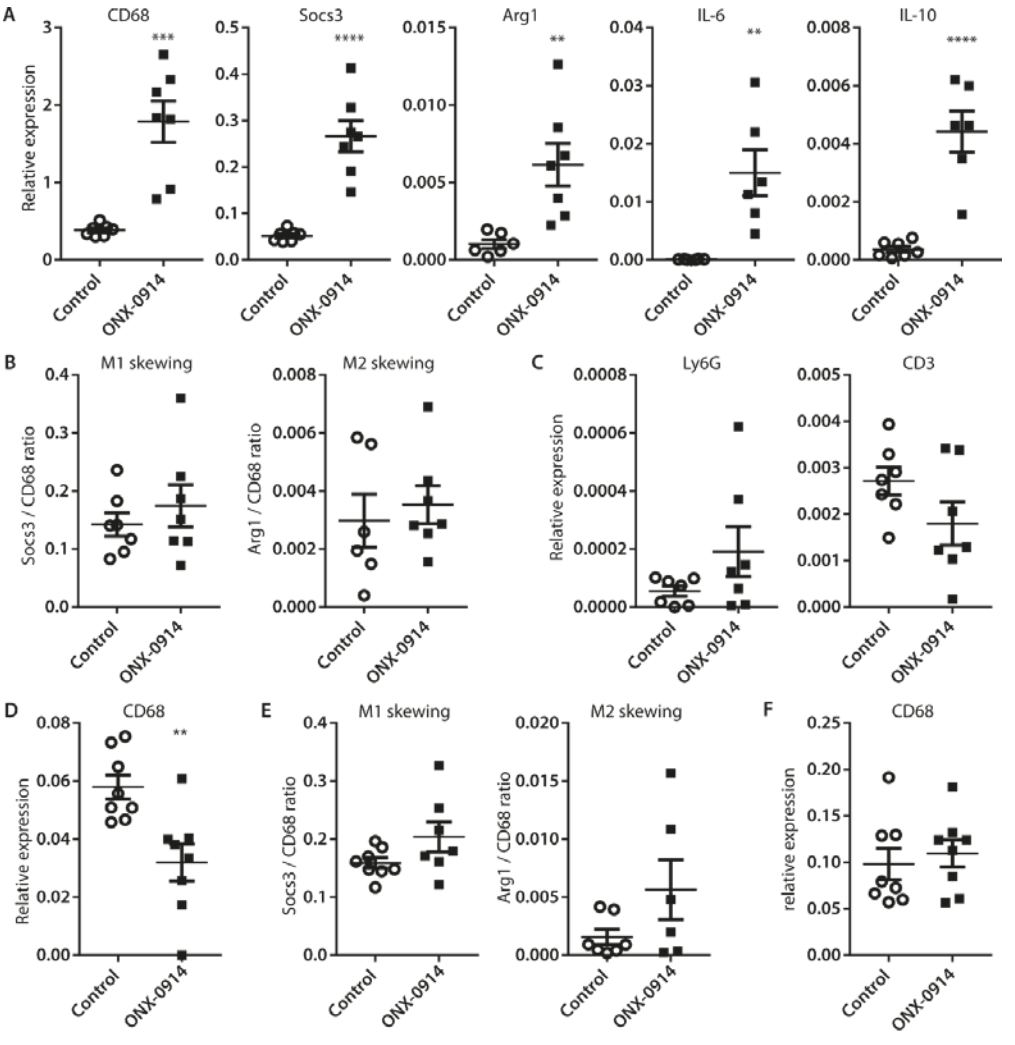

Supplementary Fig. S11 ***Macrophage infiltrate in gWAT is WAT specific and unskewed. A****) Gene expression of macrophage related genes in gWAT.* ***B****) Ratios of gene expression of M1 marker suppressor of cytokine signaling 3 (Socs3) and M2 marker arginase-1 (Arg-1) with macrophage marker CD68 in gWAT and* ***E****) interscapular BAT (iBAT). (****C****) Gene expression of Ly6G (neutrophils), and CD3 (T cells) in gWAT. CD68 gene expression in* ***D****) iBAT and* ***F****) liver. Expressed as mean ± SEM, two tailed t-test, **p < 0.01, ***p < 0.001, **** p < 0.0001*

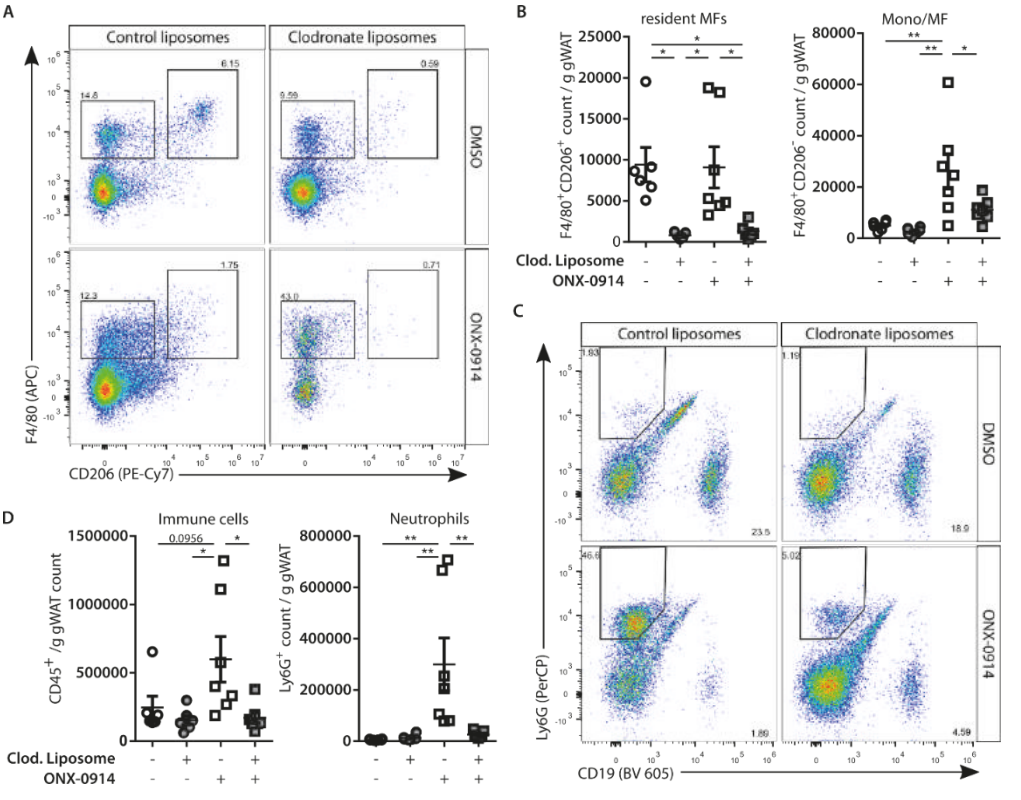

Supplementary Fig. S12 ***Depletion of peritoneal macrophages prevents macrophage and neutrophil infiltrate in gWAT.*** *gWAT from mice on WTD for 24 weeks and treated only in the final week was excised, digested and the SVF was isolated for flow cytometric analysis.* ***A****) Representative flow cytometry plot of live single CD45⁺ cells gated for F480⁺CD206⁺ resident macrophages and F480⁺CD206⁻ infiltrating macrophages* ***B****) Quantification of resident and infiltrating macrophage levels.* ***C****) Flow cytometric gating of Ly6G⁺ neutrophils in SVF, and (****D****) quantification of overall CD45⁺ immune cells and neutrophils in SVF of gWAT. Expressed as mean ± SEM, One-way ANOVA with Holm-Sidak posttest, *p < 0.05, **p < 0.01.*

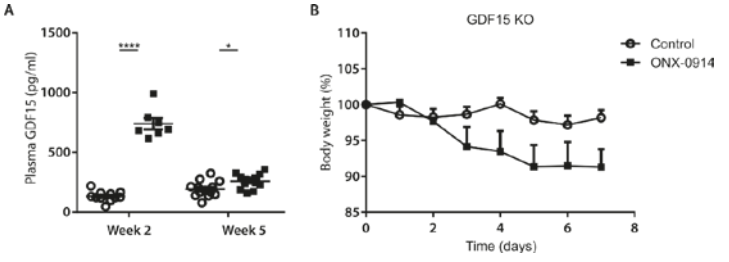

Supplementary fig. S14 ***GDF15 is induced by ONX-0914 but is not the cause of ONX-0914 induced weight loss. A****) GDF15 levels in blood plasma from two time points of the initial atherosclerosis study as assessed by ELISA.* ***B****) GDF15$^{-/-}$ mice (n=3/group) were fed WTD for 4 weeks after which mice were treated with ONX-0914 (10mg/kg, 3 times weekly) or control for a week, during which body weight was monitored. Expressed as mean ± SEM, One-way ANOVA with Holm-Sidak posttest, *p < 0.05, ****p < 0.0001.*

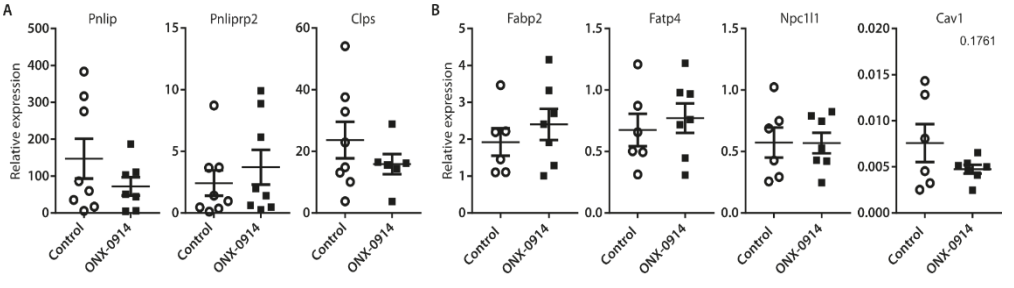

Supplementary Fig. S13 ***ONX-0914 does not affect expression of pancreatic lipases or receptors involved in intestinal lipid uptake. A****) Expression of pancreatic lipase (Pnlip), pancreatic lipase-related protein 2-like (Pnliprp2), and colipase (Clps) in pancreatic tissue isolated from female E3L.CETP mice on WTD for 5 weeks, treated with ONX-0914 for the final 2 weeks (10 mg/kg , 3 times weekly).* ***B****) Gene expression of the lipid transporters fatty acid binding protein-2 (Fabp2), fatty acid transfer protein 4 (Fatp4), caveolin 1 (Cav1), and NPC1-like intracellular cholesterol transporter 1 (Npc1l1), in intestines from female LDLr$^{-/-}$ females on WTD for 6 months, ip treated with ONX-0914 (10 mg/kg, 3 times weekly) in the final week. Expressed as mean ± SEM, unpaired two-tailed t-test, no significant data.*

Table S1**. Primers used for gene expression analysis.** Gene expression was normalized to housekeeping genes Actb and Rplp0.

Gene	Protein	Fw primer	Rev primer
Arg1	Arginase-1	tggcagaggtccagaagaatgg	gtgagcatccacccaaatgacac
Cav1	Caveolin-1	actgagaagcaagtgtatgacgcgc	cagatgccgtcgaaactgtgtgtcc
Ccl2	Chemokine (C-C motif) ligand 2	ctgaagccagctctctcttcctc	ggtgaatgagtagcagcaggtga
CD3e	T-cell surface glycoprotein CD3 epsilon chain	tctgctacacaccagcctcaaa	atgaccatcagcaagcccaga
CD68	CD68	tgcctgacaagggacacttcggg	gcgggtgatgcagaaggcgatg
Clps	Colipase	ttgcacacacaaggccatggagaa	catagttggtgttggtgatggcgc
Cyp3a11	Cytochrome P450 3A11	cccacattcaccagtggaaaactcaag	cttgcctttctttgccttctgcctc
Fabp2	Fatty acid-binding protein	cacgtgtagacaatggaaaggagctga	aatcgcttggcctcaactccttcat
Il10	Interleukin-10	gggtgagaagctgaagaccctc	tggccttgtagacaccttggtc
Il6	Interleukin-6	tgagactggggatgtctgtagctcat	gttgtcaccagcatcagtcccaaga
Ly6G	Lymphocyte antigen 6G	gatggattttgcgttgctctgga	gagtagtggggcagatgggaag
Npc1l1	NPC1-like intracellular cholesterol transporter 1	ctacacggcctggtcttcct	aaggggtactgtgggcaag
Pnlip	Pancreatic triacylglycerol lipase	tgggagcatcaaggatcacagtgga	gagacagtgtgagcaggacgtcttc
Pnliprp2	Pancreatic lipase-related protein 2	atgggagcttcacaaatcacagtgca	acgtttattatgggaagaggcacggg
Pparg	peroxisome proliferator activated receptor gamma	agggcgatcttgacaggaaagacaac	aaaattcggatggccacctctttgc
Psmb10	20S proteasome subunit beta-2i	cgtctgccctttactgcccttgg	tgatcacacaggcatccacattgcc
Psmb5	20S proteasome subunit beta-5	gcctccaaactgctcgctaacatgg	gatcctgttcccctcgctgtctacg
Psmb6	20S proteasome subunit beta-1	gaatcatcattgcaggctgggaccc	tagccatagatgtacgagctcccgg
Psmb7	20S proteasome subunit beta-2	actttcttcgtccattctcagtgccc	aaccacccacagcaccattcacg
Psmb8	20S proteasome subunit beta-5i	ttccaacatgatgctgcagtaccgg	gtggaaaacatctgtcccgagagcc
Psmb9	20S proteasome subunit beta-1i	gtgccggcgtttcaccacagat	agaattttggcagctcatctcccagg
Psme1	PA28a	tttcgctttcccttcccgct	cttgctacacaggtcttcacgga
Psme2	PA28b	ggccttgctcgctttggttaag	actctctccagcaccttctcct
Slc27a4	Long-chain fatty acid transport protein 4	ctggagagctttgcacagaccttga	ctccttccgcaactctgtcttctgg
Socs3	Suppressor of cytokine signaling 3	cccaaggccggagatttcgctt	gcgggaaacttgctgtgggtga
Ucp-1	Uncoupling protein 1	ccaagctgtgcgatgtccatgtaca	aaacatgatgacgttccaggacccg
Actb	Actin beta	cttctttgcagctccttcgttgccg	aatacagcccggggagcatcgtc
RPLP0	60S acidic ribosomal protein P0	ctgagtacaccttcccacttactga	cgactcttcctttgcttcagcttt